

A review on segmentation of knee articular cartilage: from conventional methods towards deep learning

Somayeh Ebrahimkhani^{a,*}, Mohamed Hisham Jaward^b, Flavia M. Cicuttini^c, Anuja Dharmaratne^a, Yuanyuan Wang^c, Alba G. Seco de Herrera^d

^a*School of Information Technology, Monash University Malaysia, 47500 Selangor, Malaysia*

^b*School of Engineering, Electrical and Computer Systems Engineering, Monash University Malaysia, 47500 Selangor, Malaysia*

^c*Department of Epidemiology and Preventive Medicine, School of Public Health and Preventive Medicine, Monash University, Alfred Hospital, Melbourne, Australia*

^d*School of Computer Science and Electronic Engineering (CSEE), University of Essex, Wivenhoe Park, Colchester CO4 3SQ, UK*

Abstract

In this paper, we review the state-of-the-art approaches for knee articular cartilage segmentation from conventional techniques to deep learning (DL) based techniques. Knee articular cartilage segmentation on magnetic resonance (MR) images is of great importance in early diagnosis of osteoarthritis (OA). Besides, segmentation allows estimating the articular cartilage loss rate which is utilised in clinical practice for assessing the disease progression and morphological changes. It has been traditionally applied in quantifying longitudinal knee OA progression pattern to detect and assess the articular cartilage thickness and volume. Topics covered include various image processing algorithms and major features of different segmentation techniques, feature computations and the performance evaluation metrics. This paper is intended to provide researchers with a broad overview of the currently existing methods in the field, as well as to highlight the shortcomings and potential considerations in the application at clinical practice. The survey showed that state-of-the-art techniques based on DL outperform the other segmentation methods. The analysis of the existing methods reveals that integration of DL-based algorithms with other traditional model-based approaches has achieved the best results (mean Dice similarity coefficient (DSC) between 85.8% and 90%).

Keywords:

Knee osteoarthritis (OA), Articular cartilage segmentation, Magnetic resonance imaging (MRI), Medical image analysis, Deep convolutional neural network (CNN)

1. Introduction

Osteoarthritis (OA) is by far the most common musculoskeletal disease and one of the leading causes of pain and functional disability in joints among a middle-aged and elderly population around the globe [1]. Clinically, OA has been characterised by the degenerative and structural changes in joint tissues, including bones and their corresponding cartilages [1]. Knee and hip are joints mostly affected by OA, wherein knee and hip OA have contributed substantial burden to the global disability and health resources [1, 2]. In 2014, the years of life lived with disability estimation, particularly for hip and knee OA, had been ranked the 11th highest contributor of global disability listed by the World Health Organization (WHO) [1]. Apparently, OA is more prevalent in women than in men [1], and its occurrences are expected to escalate due to the ageing of the population and the obesity epidemic in the upcoming decades [3].

Up to the present day, the cure for OA has yet to be discovered and the contributory factors for the development and progression of this disease have yet to be well-understood [4, 5]. In knee and hip OA cases, the advanced stage of OA often results in total knee replacement and total hip replacement surgeries [1, 6]. Notably, the demand for total knee joint replacement surgery (JRS) has been predicted to hike by as much as 673% by 2030 [7], thus contributing

*Corresponding author

Email address: somayeh.ebrah@monash.edu (Somayeh Ebrahimkhani)

to a substantial amount of healthcare budget and resources attributable to OA [1]. The costs of the disease have to be considered in terms of hospitalisation [8], healthcare utilisation within the 2-year preceding surgery [9], and JRS [10, 11]. The average direct cost of OA per patient, primarily due to JRS, was estimated to vary from \$577 to \$811 and from \$1,422 to \$21,355 in Canada [10] and the United States [11], respectively.

1.1. Imaging modality and articular cartilage quantification

A very wide range of imaging modalities are now available in healthcare and biomedical research in the understanding of OA pathogenesis [12, 13]. Choice of a particular imaging technique depends on the possible role of each modality in recognising various structural changes and different OA-associated tissue damages in knee joint including articular cartilage, synovitis, subchondral bone, and menisci. Computed tomography (CT) offers an excellent three-dimensional visualisation when imaging cortical bone, osteophytes, and soft tissue calcification [12, 13, 14, 15]. However, CT has its limitations; in particular, the patient is exposed to radiation [14, 16] and hence it is not widely used for the early detection of OA [16, 17]. Imaging techniques based on nuclear medicine such as positron emission tomography (PET), scintigraphy, and single-photon emission CT (SPECT) are being used for bone imaging and discriminating between bone and soft tissue [13, 16]. The poor anatomic resolution and the exposure to radiation are the main limitations of these modalities [14, 16]. Ultrasound is another imaging modality that can be used for detecting synovitis, synovial inflammation and hypertrophy in knee OA patients without exposure to the radiation [12, 15, 16] but it is more sensitive to the clinical practices (i.e., operator-dependent) [12]. Moreover, ultrasound does not provide data pertaining to the whole joint [17] and it does not have a significant role in the early detection of OA [17, 18]. Optical coherence tomography (OCT) is another imaging modality that is useful in assessing the disease state and monitoring the thickness changes of articular cartilage in OA patients [12]. Limitation of OCT imaging is that it is an invasive procedure and an operator-dependent technique [12].

Radiography is the most commonly used imaging biomarker for OA in both clinical and epidemiological settings [18, 19]. Radiography enables the direct assessment of the bony structure, such as osteophytes and subchondral cysts, as well as indirect assessment of the articular cartilage using joint space width [18, 19, 20]. Nonetheless, it is incapable of (i) depicting soft tissues; (ii) direct visualisation of cartilage; and (iii) monitoring disease progression sufficiently [20, 21]. The OA is a disease that progresses very slowly and radiography limits the ability to diagnose the presence of structural changes of the whole joint and disease symptoms. This makes radiography infeasible in assessing cartilage loss and to detect small changes of the whole joint for a long period [19, 20].

Among various imaging modalities mentioned above, an ideal imaging modality should: (1) visualize the whole joint structure, including direct visualization of bone and cartilage three-dimensionally, (2) discriminate various tissue types with a higher anatomical resolution, (3) be highly sensitive to structural changes in OA patients without exposure to radiation, and (4) be non-invasive. Magnetic resonance imaging (MRI) can be used in the detection of OA in symptomatic patients fulfilling many of these criteria [22]. MRI is usually the modality of choice for structural analysis and quantification of changes in the whole joint and specifically cartilage tissues, and additionally permits better visualisation of cartilage morphology [18, 19]. Further, MRI offers a high contrast of soft tissues for assessment of cartilage damage and is substantially accurate and sensitive to morphological changes [19, 21]. Thus, MRI can directly visualise the cartilage and enables semi-quantitative and quantitative morphologic assessments of cartilage [18, 19].

Different magnetic resonance (MR) sequences are used for qualitative evaluation or morphological assessment of the cartilage [18, 22]. Table 1 reports the most adopted MR sequences for morphological assessment of cartilage and bone including qualitative and quantitative evaluations along with their strengths and drawbacks. Various MRI parameters affect the contrast level between synovial fluid and cartilage. Fat suppression (FS) is a technique that allows an excellent depiction of cartilaginous defects and provides a high contrast at bone-cartilage interface (BCI) [22]. The most common musculoskeletal clinical imaging techniques are widespread on MRIs, such as proton density (PD) weighted, T1-, and T2-weighted with fat-suppressed imaging that is used in the morphological assessment of knee articular cartilage [12, 18, 22]. The strength of the magnetic field in knee MRIs is another influencing factor that can contribute to improved clinical performance because of the higher signal-to-noise ratio (SNR) of an MR scanner. Theoretically, SNR is approximately linearly related to the magnetic field strength [23]. Higher SNR and increased contrast of the cartilage tissue to surrounding tissues, such as the bone, meniscus, and synovial fluid, is observed at 3-Tesla (3.0 T) MR scanner than that of an MR scanner with the most commonly used 1.5 T magnetic field strength in clinical standard [23, 24]. The use of an MR sequence with higher magnetic is believed to result in

an improved MR-derived structural and morphological detectability for the articular cartilage and allows an accurate assessment of cartilage volume and thickness [25, 24]. Recently, ultra-high-field 7T MRIs of the knee has received considerable attention to hasten early detection of damaged cartilage [24, 26]; however, there are some technical challenges including larger B1 inhomogeneity, transmitted RF energy, and excessive heating of tissue [24]. In general, 3D spoiled gradient-echo (SPGR) imaging is the standard imaging technique for an accurate quantitative assessment of knee articular cartilage [22, 27]. In addition, SPGR-type imaging achieves a high resolution 3D images, providing a high SNR, shorter acquisition time, and better synovial fluid-cartilage contrast [22].

Table 1: Different MR sequences for cartilage quantification adopted from [18, 22]. Acronyms are from left to right (in order of appearance): two-dimensional (2D), proton-density (PD), fast spin-echo (FSE), partial volume effect (PVE), three-dimensional (3D), signal-to-noise ratio (SNR), knee osteoarthritis (KOA), sampling perfection with application-optimized contrast using different flip-angle evolutions (SPACE), spoiled gradient-echo (SPGR), bone cartilage interface (BCI), dual-echo steady-state (DESS), balanced steady-state free precession pulse (bSSFP), driven equilibrium Fourier transform (DEFT).

MR sequence	Usage	Type of information	Strength	Drawback
Qualitative				
2D PD FSE	2D cartilage imaging	Cartilage signal intensity	High contrast between synovial fluid and cartilage, short scan time	Anisotropic voxels, section gaps, PVE
3D FSE	3D cartilage imaging	Cartilage thickness	Isotropic resolution, low possibility for PVE, high SNR	Not yet applied in KOA trials, edge blurring
3D FSE SPACE	3D bone imaging	Subchondral lesions characterization	Isotropic resolution, high SNR	Long scan time, not yet validated for assessment of cartilage lesions
Quantitative				
T1-3D SPGR	3D cartilage imaging	Cartilage volume	Isotropic resolution, low possibility for PVE, suitable for cartilage imaging, good contrast of BCI in 3D	Long scan time, unable to assess marrow abnormalities, poor contrast between synovial fluid and cartilage
3D DESS	3D cartilage imaging	Cartilage volume	High contrast between synovial fluid and cartilage, short scan time, high SNR, isotropic resolution, the low possibility for PVE, allows total cartilage representation	Unable to assess marrow abnormalities, high sensitivity to artefacts

Continued...

Table 1 Continued. . .

MR sequence	Usage	Type of information	Strength	Drawback
3D bSSFP	3D cartilage and bone imaging	Area of cartilage surface and subchondral bone, cartilage thickness	High SNR, high contrast between synovial fluid and cartilage, suitable ligaments and menisci imaging, isotropic resolution, low possibility for PVE	Not yet applied in KOA trials
3D DEFT	N/A	The denuded area	Diagnostic performance similar to 2D FSE and SPGR sequences, high contrast between synovial fluid and cartilage	Long scan time, unable to assess marrow abnormalities, not yet utilized in KOA assessment

Semi-quantitative morphometric assessments are performed via commonly used scoring systems, such as the Knee Osteoarthritis Scoring Systems (KOSS) [28], the Boston Leeds Osteoarthritis Knee Score (BLOKS) [29], MRI Osteoarthritis Knee Score (MOAKS) [30], and the Whole-Organ MRI Score (WORMS) [31]. On the other hand, quantitative morphometric techniques exploit the three-dimensional (3D) MRI data to assess the parameters of cartilage tissue, such as volume of the cartilage (VC), area of the cartilage surface, total area of the subchondral bone (tAB) and cartilage thickness (ThC) as an OA biomarker, to evaluate the severity and the progression of OA [5, 18, 19, 32].

To obtain the above quantitative measures, the BCI and the relevant cartilage surface need to be segmented by a trained observer with assistance from specialised image analysis software to compute the articular cartilage morphometric parameters [5, 18, 33]. Nevertheless, regardless of the competence of the trained readers or the capability of segmentation software, the process of manual/semi-automatic segmentation technique is rather intricate and time-consuming [18], mainly due to several factors. Two essential considerations, particularly for longitudinal assessment of the knee compartment morphology, are the variation of knee position and the spatial resolution (section thickness, in-plane resolution) during serial acquisitions [5, 33]. In addition to spatial resolution variations, the contrast level of inter-cartilage structures (i.e., “abutting cartilage surfaces”) and its contrast with adjacent structures (synovial fluid, synovial tissue, intra-articular fat, and menisci) are some challenges in delineating the different interfaces with single contrast MRI sequences [33]. After eliciting these challenges, Kumar et al. [23] listed some other challenges in detail, such as articular cartilage structure, the modality of MRI sequences, magnetic field strength, and image artefacts.

Figure 1 illustrates a general pipeline of quantitative measurement of cartilage in both clinical and research settings. The procedure includes MRIs acquisition, pre-processing of MRI data via image processing techniques (noise removal, normalisation, etc.), extracting cartilage surface manually or automatically with advanced image analysis tools, quantitative measurement of cartilage thickness and volume, and finally, grading the severity of OA and disease status. The estimation of VC (i.e., the volume of cartilage) is computed from the product of cartilage surface area and cartilage thickness [5, 32]. Therefore, an accurate and robust segmentation technique of cartilage surface from MRI is a prerequisite in measuring changes in cartilage morphology.

1.2. Related work

Multiple reviews have focused on quantitative assessment and segmentation of articular cartilage morphology using MRI. The first review in the field was done by Eckstein et al. [5] targeting at the morphological assessment of cartilage and it was limited to several semi-automatic segmentation techniques with limited detail. Peterfy et al. [33] gave a state-of-the-art review of MRI protocols for whole-organ assessment of knee cartilage. They discussed the impact of various factors and some essential considerations, such as in-plane acquisition, section plane selection, as well as image quality in the optimal delineation of articular cartilage and its morphological assessment. In 2011, Roemer et al. [18] presented a comprehensive review of the role of different imaging modalities in semi-quantitative

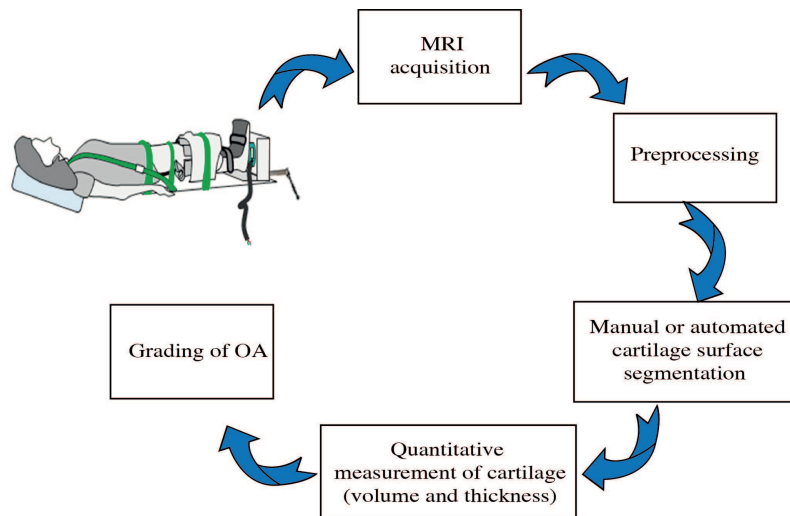


Figure 1: The general workflow of knee cartilage quantification in clinical and research settings. The schematic acquisition figure of female patient adopted with permission from [34]. Copyright 2015 by the Journal of Biomechanics.

and quantitative assessments of articular cartilage. These studies mainly focused on MRI modality and morphological assessments, instead of segmentation techniques.

A number of review articles on knee joint segmentation have been published in recent years [35, 36, 37, 38]. Arovitola and Gallo [35] and Zhang et al. [38] looked into knee bone segmentation, whereas only Zhang et al. [38] covered segmentation strategies of articular cartilage, but without a quantitative comparison of the methods. Other work in knee articular cartilage segmentation probed into segmentation strategies based on the level of automation and only covered a subset of methods [23, 37]. Kumar et al. [23] quantitatively reviewed semi-automatic and automatic methods in summary tables with limited detail and scope but lacked an analysis of results. Due to the recent advances in medical image analysis using deep learning (DL) [39], it has become a popular method for feature representation for automated segmentation of knee articular cartilage. In this way, one can learn the features from raw data without the need of a hand-crafted feature extraction technique [40]. Nevertheless, to the best of the authors' knowledge, no review article has covered DL methods applied on knee joint automatic segmentation.

1.3. Review process

A significant body of work has been published in the area of knee articular cartilage segmentation, and it is not easy to review without adopting a systematic approach to narrow down the most relevant work related to this topic. This section explains the system adopted for this purpose. Although there are many related surveys as discussed in Section 1.2, the most recent ones are the work by Kumar et al. [23] and Kubicek et al. [37], in which different techniques for the knee articular cartilage segmentation are reviewed based on automation level. However, their surveys differ from ours in the following two aspects: (i) they have not provided a comprehensive survey on all available methods applied on knee articular cartilage segmentation. (ii) In addition, DL methods are not explicitly explained and not included in [23, 37], and this is one of the key contributions of our survey. Figure 2 depicts a taxonomy of knee articular cartilage segmentation method obtained from our review process. We have classified and discussed each category in the following sections.

Following databases were used during the review: IEEE Xplore, PubMed, Scopus, Science Direct, ISI Web of Knowledge, and Google Scholar. The search term used was “Knee articular cartilage” AND (“Magnetic resonance imaging” OR “MRI”) AND “Segmentation”. We included the articles published in peer-reviewed journals, book chapters, conferences and symposiums. Additionally, we examined the reference lists of the selected publications, and the related work was included in order to retrieve other relevant publications. We excluded some articles based on the titles that were not relevant to our study. After removing duplicate entries and considering only the extended version of articles, the review has resulted in a total of 112 studies. Figure 3 shows the four-step process used to identify articles based on inclusion-exclusion criteria. Our study covered related work from the year 1994 till now.

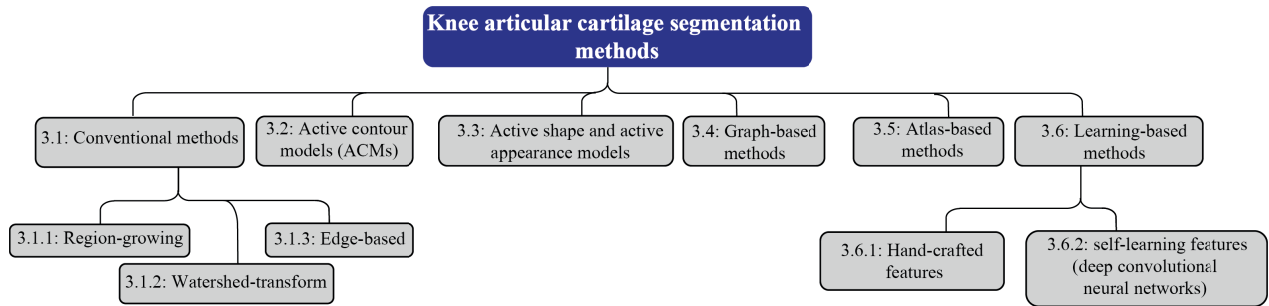


Figure 2: A taxonomy for knee articular cartilage segmentation methods.

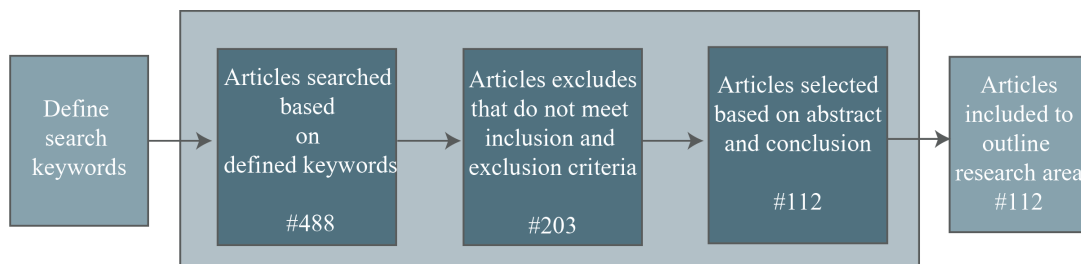


Figure 3: Article identification process.

1.4. Contributions and organization of this article

The contributions of this study are given as follows:

1. This paper presents an extended analysis of articular cartilage segmentation methods and takes it to the next level of details with a focus on algorithmic aspects by breaking down the methods into their building blocks.
2. Compared to other surveys, this is the first survey which covers the application of DL techniques for the knee cartilage segmentation problem.
3. Unlike other studies, we do not limit ourselves on the presentation of reviewed studies, but also present the quantitative results and compare them to determine their potentials and limitations.
4. Finally, specifically with learning-based approaches, we believe that feature extraction plays a significant role as it influences the learning process significantly. Unlike other studies, we have devoted a separate section on learning-based techniques to provide a detailed description of the related methods and to discuss the topic thoroughly.

The rest of this review is divided into three sections. Section 2 presents an overview of the existing methods used for knee articular cartilage segmentation. This section also explains briefly on datasets used and abbreviation used in this work. Section 3 reviews the most commonly used algorithms in knee joint segmentation, including DL methods in Section 3.6.2. Based on the existing approaches, Section 4 discusses potential future directions related to knee joint segmentation together with concluding remarks.

2. Overview

Over the past 25 years, medical image analysis techniques have been one of the most popular research topics in the field of computer vision. A substantial number of methods have been proposed for accurate delineation and quantification of knee articular cartilage. This section presents an overview of the segmentation methods that have been introduced to achieve this goal. As shown in Figure 4, this survey covers conventional techniques like region-growing to model state-of-the-arts, DL-based techniques. Segmentation methods based on the required user interaction could be categorised into: *interactive*; *semi-automatic*; or *fully automatic*. These techniques have been described in the subsequent sections.

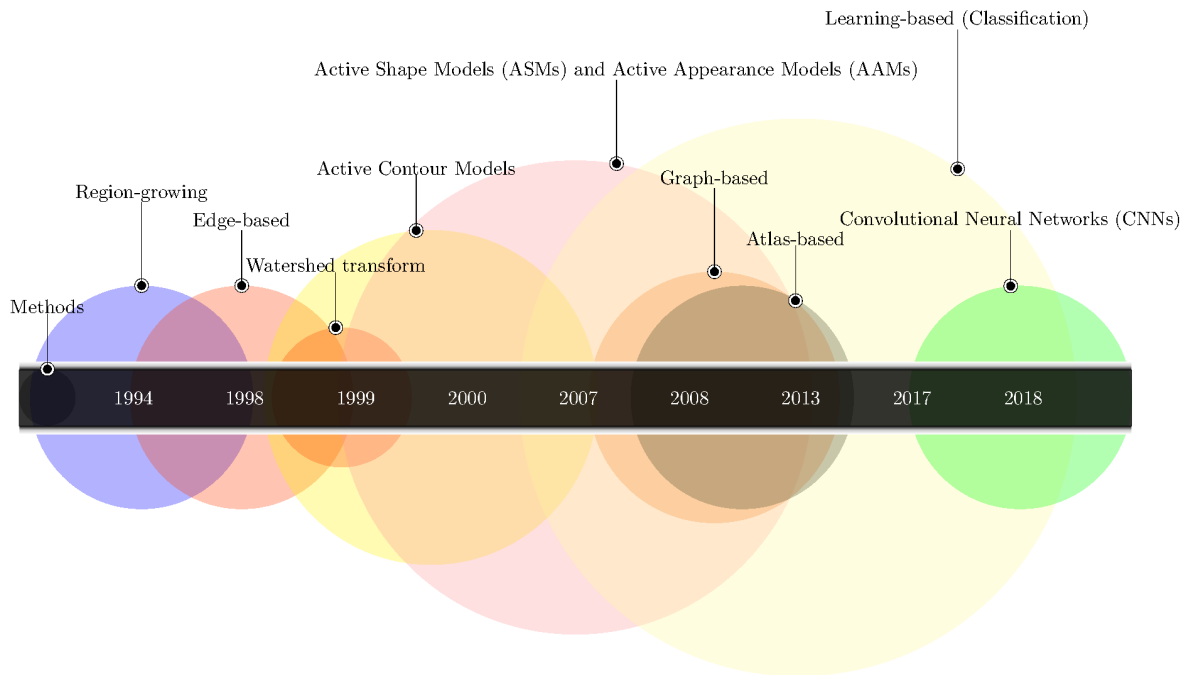


Figure 4: Historical timeline of medical image analysis methods used for segmentation of knee articular cartilage; the radius of circles represents the quantity of works utilising a specific method.

The conventional segmentation strategies are simple yet often useful methods that segment images based on homogeneity of intensity/texture and similarity criterion in a region [41]. Conventional segmentation methods are based on the idea that objects have quantifiable attributes, such as pixel intensity and gradient magnitude information (i.e., edge information). Such segmentation techniques can be categorised into region-growing, edge-based, and Watershed transform (WST) techniques. In 1994, Peterfy et al. [42] tested region-growing method for segmentation of articular cartilage to assess inter- and intra-observer reproducibility, and to validate MRI-based quantification. Concurrently, several other studies began using edge-based [43] and WST [44] segmentation methods using edge data as the criterion to segment articular cartilage. Active contour models (ACMs) [45] and active shape models (ASMs) [46] which were also introduced at the same time, are by far the most often used methods to segment articular cartilage. The application of ACMs and ASMs is considered as model-driven techniques that integrated high-level knowledge, such as variation in shape and appearance [47, 41].

One popular approach for segmentation of articular cartilage is graph-cuts (Gcuts) that are commonly applied for automatic or semi-automatic segmentation. In 2008, Gcuts were used for semi-automatic segmentation of articular cartilage [48]. Atlas-based segmentation is another popular method widely used in this domain [49]. With the rising popularity of machine learning techniques in medical image classification and segmentation, much of the literature has been focused on classification algorithms to discriminate cartilage pixel/voxel from non-cartilage one. In 2005, k -nearest neighbor (k NN) was employed to classify cartilage voxels [50]. More recently, with advances in DL, some studies have proposed the use of deep convolutional neural networks (CNNs) for knee tissue segmentation to automatically learn features. Before the segmentation methods are reviewed in Section 3 in detail, a brief description of datasets and performance metrics used for evaluation are provided in the following paragraphs.

A comparison of the different segmentation methods is not a trivial task. There are a few publicly available databases manually labelled and they are to be served as ground truth data. However, some authors have used their own “in-house” MRIs for evaluation, which make the quantitative comparison of studies infeasible. As we have noticed from the reviewed articles, Medical Image Analysis for the Clinics (MICCAI) challenge on Segmentation of

Knee Images 2010 (SKI10)¹ and the Osteoarthritis Initiative (OAI)² are the most frequently used public databases. In this paper, we review the state-of-the-art approaches for knee articular cartilage segmentation with a focus on the application of these algorithms and their performances in these two public datasets. MICCAI challenge in knee structure segmentation has been introduced [51] to allow the participants in the challenge to compare the overall strategies in terms of average segmentation error for each structure (i.e., bone and cartilage) independently.

Apart from the difference in the used database, the results are evaluated and presented in different ways in the reviewed papers. Moreover, there is no standard measure for evaluation, thus the segmentation results are reported using different evaluation metrics. Based on the analysis of literature, most of these evaluation metrics are based on either the distance or volume overlap. The most common quantitative measures used for knee MRI segmentation methods are tabulated below as shown in Table 2. The most commonly used evaluation measure among those based on volume overlap, is Dice similarity coefficient (DSC) [52]. For this reason, regardless of the dataset used, DSC is the main criterion for comparison in this work. The root-mean-square symmetric surface distance (RMSD), volume difference (VD), and volume overlap error (VOE) metrics from MICCAI scoring system [53] are used for bone and cartilage segmentation. Other metrics are also used to evaluate the accuracy of knee cartilage segmentation algorithm such as specificity (SP) and sensitivity (SN). Some metrics used in this article rely on distance measure to compute how far the boundaries of segmentation results are from the ground truth such as the Hausdorff distance (HD). Distance measures are provided in millimetres (mm). Throughout the reviewed literature, the term reproducible usually tends to be used to examine the results under same circumstances, which means whether the measurement of a phenomenon is the same upon repeating a specific procedure or not. Root-mean-square error (RMSE) and coefficient of variation (CV) are two main metrics used to measure the reproducibility of segmentation algorithms [19]. These measurements can be calculated on the following knee compartments which are abbreviated using symbols as listed below in Table 3. Figure 5 shows a typical T1-weighted MRI obtained from one patient and the corresponding segmentation of articular cartilage surfaces with annotated bones. Three-dimensional reconstruction of articular cartilage surfaces from two views (medial and lateral sides) of the same patient is presented in Figure 6.

Table 2: A summary of popular quantitative measure for knee articular cartilage segmentation and their mathematical formulation. Within the following formulas, A denotes the manual segmentation results by experienced radiologists is used as gold standard to be compared to the segmentation results obtained by the algorithm, B ; ∂A and ∂B are the surface of objects of the gold standard and segmentation algorithm, respectively; $n_{\partial A}$ and $n_{\partial B}$ are the number of voxels on the surface of A and B ; V and $d(a, \partial B)$ denote a volume and the nearest Euclidean distance of a surface point a on ∂A to the boundary ∂B ; acronyms are: false positives (FP), true positives (TP), false negatives (FN), true negatives (TN), standard deviation (σ), mean (μ), error between ground truth and segmentation result of the subject i (e_i).

Metrics	Mathematical description
Dice similarity coefficient (DSC)	$DSC = \frac{2V_A \cap V_B}{V_A + V_B}$
Volumetric overlap error (VOE)	$VOE = 100 \cdot \left(1 - \frac{DSC}{200 - DSC}\right)$
Volumetric difference (VD)	$VD = 100 \cdot \frac{V_B - V_A}{V_A}$
Specificity (SP) or true negative rate	$SP = \frac{TN}{TN + FP}$
Sensitivity (SN) or true positive rate	$SN = \frac{TP}{TP + FN}$
Hausdorff distance (HD)	$HD = \max\{sup_{a \in \partial A} d(b, a), sup_{b \in \partial B} d(a, b)\}$
root-mean-square symmetric surface distance (RMSD)	$RMSD = \sqrt{\frac{1}{n_{\partial A} + n_{\partial B}}} \cdot \sqrt{\left(\sum_{a \in \partial A} d^2(a, \partial B) + \sum_{b \in \partial B} d^2(b, \partial A)\right)}$
Root-mean-square error (RMSE)	$RMSE = \sqrt{\frac{1}{n} \sum_{i=1}^N e_i^2}$
coefficient of variation (CV)	$CV = 100 \cdot \frac{\sigma}{\mu}$

¹<http://www.ski10.org/>

²<https://oai.epi-ucsf.org/datarelease/>

Table 3: Description of knee compartment notations.

Knee bone surface	Symbol	Knee cartilage surface	Symbol
Femur bone	bF	Total femoral cartilage	cF
		Medial femoral cartilage	cMF
Tibia bone	bT	Total tibial cartilage	cT
		Medial tibial cartilage	cMT
		Lateral tibial cartilage	cLT
Patella bone	bPT	Patellar cartilage	cPT

3. Knee articular cartilage segmentation methods

This section discusses the most commonly used techniques in knee articular cartilage segmentation, dividing them into six categories (see Figure 2).

3.1. Conventional segmentation methods

Conventional segmentation strategies, such as region-growing, Watershed transform, and edge-based, have been mostly performed in an interactive and slice-wise scheme. As explained in Section 2, object segmentation is mostly performed based on some common criteria such as homogeneity of intensity/texture in a region. Conventional segmentation strategies integrate data and domain knowledge for the segmentation process. Domain knowledge (i.e., information about the object to be segmented) is integrated interactively into conventional segmentation techniques [41]. Most of these methods requires an intermediate level of user interaction (i.e., semi-automatic).

According to the previously done review in [54], conventional segmentation strategies fall into the same category of *thresholding-based algorithms*. Note that a similar grouping strategy was adapted to categorise the knee articular cartilage segmentation methodologies in this paper.

3.1.1. Region-growing

This method extracts connected regions, and groups pixels into a larger region based on a predefined similarity criterion [41, 55]. Similarity criterion is based on the homogeneity of features, such as grey-level intensity, texture, and edge [47, 55]. An initialisation point for segmentation, known as a seed point, is manually placed by a user to extract all pixels (regions) connected to the initial seed point to fulfil the predefined criteria (i.e., a homogeneity condition) and merge them based on the similarity criteria [47, 56]. The idea is to expand the seeded region by merging and classifying the neighbouring pixels into regions [41].

A number of early studies adopted *seeded region-growing* [57] to delineate cartilage area [58, 59, 60, 61, 62, 63, 64, 65, 66], whereby the seed point is placed manually in the centre of the cartilage. Although this technique has been widely used in the past two decades, it is prone to the local variation of intensity. Pakin et al. [66] conducted region-growing, followed by voxel labelling as cartilage/non-cartilage (i.e., two-class intensity-based local clustering), and then, 3D deformable models for cartilage separation to tackle the issue of intensity inhomogeneity. Although region-growing segmentation is interactively performed either in the form of manual initialisation or cartilage border delineation, inclusion of prior anatomical knowledge, such as the closeness of cartilage and bone tissue, helps to minimise user interaction in the extraction of initial cartilage. For instance, 3D Euclidean distance transform (EDT) from the femur and tibia bone (bT) regions were computed to extract the boundary of the cartilage [65, 66].

Nonetheless, leakage of intensity to the background due to noise and low contrast between the anatomical structures are some drawbacks that may constrain the initialisation of segmentation, thus making segmentation rely on various parameters. To solve these shortcomings, Tamez-Peña et al. [67] analysed region-growing and region merging via Mumford-Shah optimisation variational approach [68]. In this method, a cost function is defined to initialise the parameters for the region-growing algorithm so that the optimisation process ends with lower minima of the cost function.

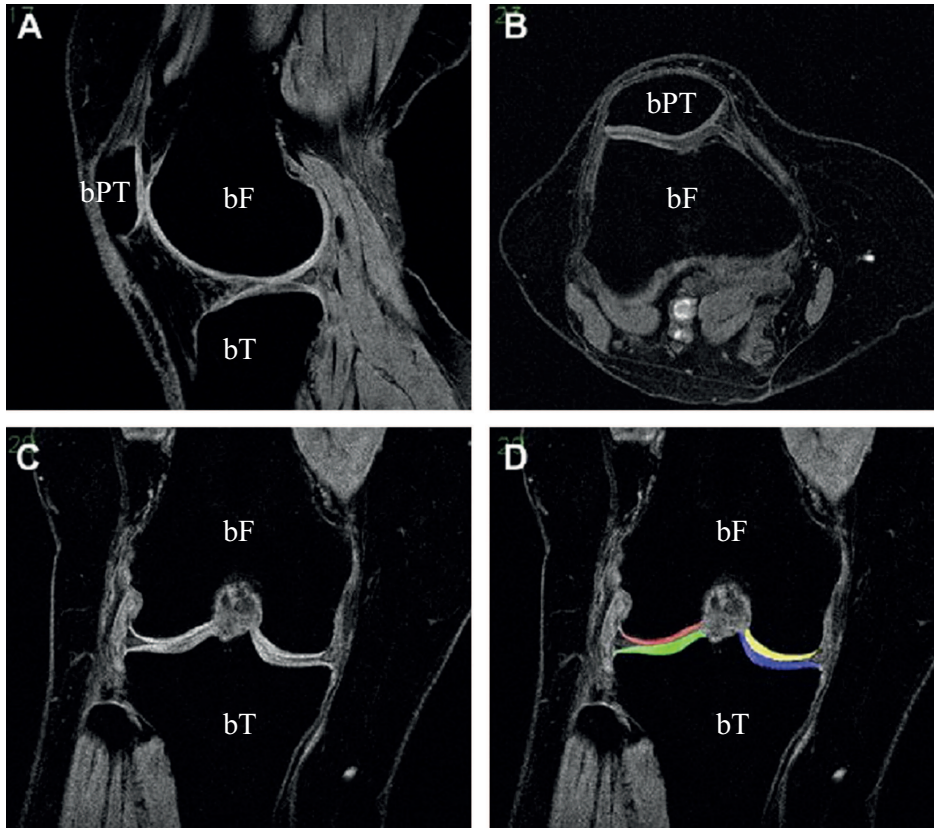


Figure 5: A sample knee MRI obtained with spoiled gradient-echo (SPGR) sequences with water excitation (WE) is shown as (A) sagittal view; (B) axial view; (C) coronal view; (D) coronal view with corresponding manual anatomical labels. The colours for the manual labels correspond to the different knee bone and articular cartilage compartments: The medial tibial cartilage (cMT) labelled blue, lateral tibial cartilage (cLT) labelled green, medial femoral cartilage (cMF) and lateral femoral cartilage (cLF) labelled yellow and red, respectively. Knee bones marked as femur bone (bF), tibia bone (bT), and patella bone (bPT). Copyright 2014 by the Best Practice & Research Clinical Rheumatology. Reprinted and adapted with permission from [16].

3.1.2. Watershed-transform (WST)

Watershed-transform (WST) is a hybrid method that incorporates image gradient information (i.e., edges) and mathematical morphology as the criteria to separate articular cartilage from its surrounding tissues [44, 69]. WST can be applied to an intensity image or gradient magnitude image, in which the value of gradient magnitude is treated as the height or altitude [41]. The intuitive idea underlying this method is that different regions in an image are assumed to be catchment basins (i.e., the local minimum in the image plane), which get flooded with water (i.e., grey level value) [41, 70].

The immersion-based WST is a primary approach to implement WST segmentation [71]. This algorithm is based on immersing slowly the local minimum points (i.e., pixels with minimum intensity or gradient magnitude in a basin) into water. The rising water in the basin is merged with the segment from its surrounding basins so that the points with the highest gradient magnitude (i.e., edges) will stop the immersion process. This procedure results in a region surrounded by the object boundary. Gosh et al. [44, 72, 73] successfully applied the immersion-based WST segmentation technique to differentiate OA population from healthy subjects and to minimise user interactions compared to region-growing techniques. The algorithm is performed with varied pixel intensity, spatial proximity, detection of local minima, and clustering. First, low-pass filtering is applied on images to correct the intensity inhomogeneities. Next, WST segmentation is used to generate the cartilage boundary. In 2004, Grau et al. [69] proposed a modification to the conventional WST algorithm by including the variance of class probabilities between two neighbouring pixels as the prior knowledge in WST. The user manually places one marker for each of the three classes (i.e., bone, carti-

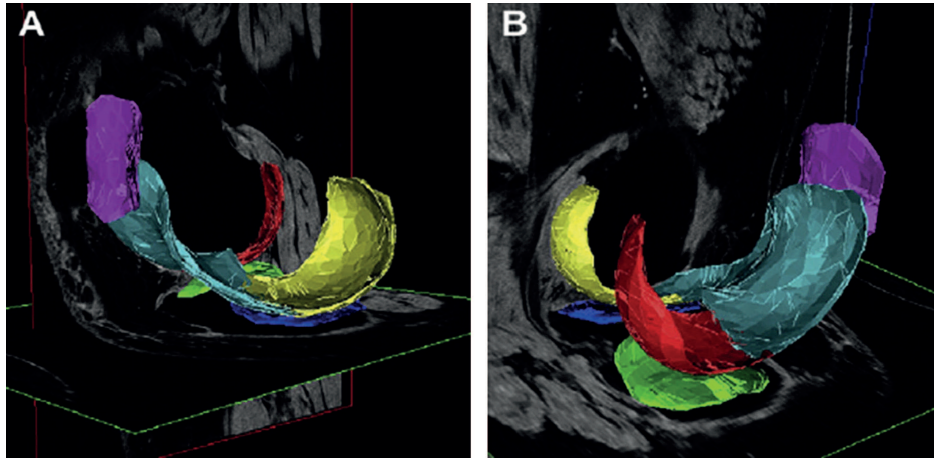


Figure 6: Volumetric representation of knee articular cartilage surfaces. The sagittal view of knee MRI is visualised on both (A) medial and (B) lateral sides. Each colour represents a specific knee articular cartilage plates: the medial tibial cartilage (cMT) labelled blue, lateral tibial cartilage (cLT) labelled green, medial femoral cartilage (cMF) labelled yellow, lateral femoral cartilage (cLF) labelled red, femoral trochlear cartilage labelled turquoise, and patellar cartilage (cPT) labelled magenta. Copyright 2014 by the Best Practice & Research Clinical Rheumatology. Reprinted with permission from [16].

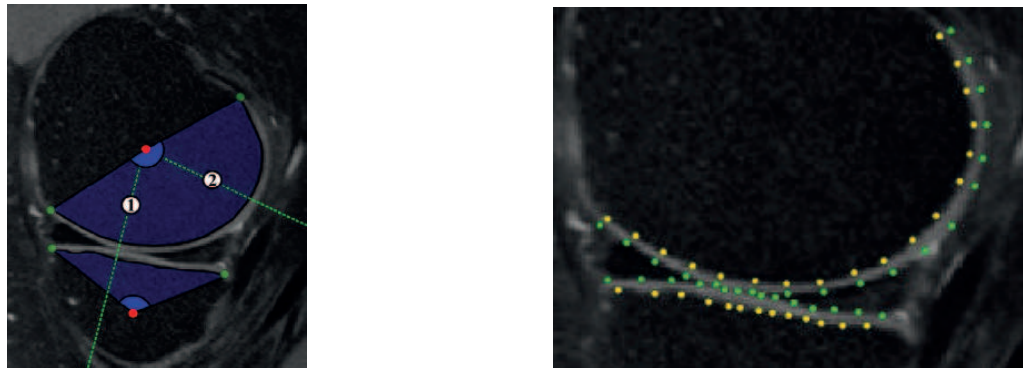
lage, and other tissues), while Markov random fields (MRF) [74] offer the local correlations between a pixel and its neighbours.

The issue of over-segmentation while using WST is also worthwhile to be explored. Image noise and sensitivity to the local variation of intensity necessitate image pre-processing and post-processing to decrease the risk of over-segmentation. Ghosh et al. [44, 72, 73] utilised an intensity-based connectivity cross-correlation to minimise over-segmentation artefacts. Fluctuation in the gradient magnitude image can cause over-segmentation. A few methods have been proposed to address these issues; among them, Grau et al. [69] applied several local minima gradient points as markers to propagate the labelling process of the neighbouring pixels, wherein the local minima of neighbouring pixels contribute to a kind of arbitrary assignment of labels. This may cause biased segmentation. Hence, an algorithm that visits the neighbouring voxels in an invariant order (i.e., order-invariant) might be a feasible approach to address the issue of biased segmentation results. Besides, the pre-processing steps, such as geodesic reconstruction, can address over-segmentation problem [70]. In 2006, the method proposed in [75] has corrected the voxel-wise classification by combining the posterior probability map of the classification step with WST.

3.1.3. Edge-based

Edge-based algorithms refer to another category of conventional segmentation techniques, in which the gradient magnitude of intensity can separate various textures. Most of the segmentation techniques based on edge detection are rarely applied alone but are used in conjunction with other methods. These methods are generally composed of three steps: pre-processing, edge detection, and post-processing. Therefore, potential pre-processing and post-processing steps have received much attention in edge-based techniques. The pre-processing step is responsible for cleaning the MRIs from noise and artefacts. Among different edge detection algorithms, Canny edge detector [76] has been widely used to delineate cartilage boundaries using the gradient magnitude. Edge detection significantly reduces the size of image data and filters out useless data (i.e., noise influence). Nevertheless, discontinuities may occur within the potential edge pixels due to the high gradients of noise, which necessitates one to correct object boundaries manually in the post-processing step. Boundaries can be corrected by applying spline curve fitting or morphological operators to connect cartilage discontinuities. Swamy and Holi [77, 78] proposed an edge-based method for cartilage segmentation that starts with image pre-processing. First, median filtering was performed to remove noise from MRI. Second, upon detecting edges via Canny edge detection, control points are manually placed on knee cartilage boundary to mark the inner and outer regions of the articular cartilage. The B-spline curve-fitting method is used to interpolate the salient points.

In some other frameworks [79, 80], noise reduction and region-of-interest (ROI) detection are performed simulta-



(a) An illustration of the radial search method illustrating reference and edge,

(b) Inner boundary points (yellow) and outer boundary points (green).

Figure 7: Segmentation based on radial search method. An example of reference and boundary points in femoral and tibial cartilage derived from an MRI slice. Copyright 2017 by the Taylor & Francis. Adopted with permission from [88].

neously. The pre-processing step selects the ROI by excluding regions with less informative contents. Cartilage edges can be enhanced by using various noise reduction methods. For instance, anisotropic diffusion algorithm, Laplacian of Gaussian (LoG), and median filtering have been employed in [78, 81, 82] prior to edge-detection. Bezier spline curve fitting was initiated by placing control points within the cartilage area. Rays vertical to the spline on the control points were followed to determine bone cartilage boundary (as shown in Figure 7) [81].

Alternatively, both inner and outer boundaries of cartilage can be extracted via radii (radial) search in some studies instead of using conventional edge detectors [83, 84, 85, 86, 87, 88]. For instance, a radial search method was performed to segment the articular cartilage area in [68]. First, a threshold value is selected, and then the algorithm is used by placing a reference point O at the centre of the femur bone along a horizontal line, called radial line, from the origin point, as illustrated in Figure 7. Radius r with a particular length is determined by a vector that begins from the reference point with angle θ from the horizontal axis to seek femur-cartilage interface (i.e., inner boundary) [84]. The coordinates and the intensity of the points along the vector are determined, and the procedure is repeated for a predefined number of radial lines and increasing angle θ each time to cover the entire femur condyle. A similar process is applied in the reverse direction to search for cartilage-synovial interface (i.e., outer boundary) (see Figure 7(b)). The angle is increased from zero to the maximum degree that covers the weight-bearing region of cartilage (see Figure 7(a)). A similar approach was applied for knee bone segmentation in [89].

A drawback of this method is due to the complicated thresholding mechanism used to create intensity profiles, especially within the soft tissue regions. This is due to the similarity of contrast levels between inter-cartilage structures and adjacent structures. Liukkonen et al. [88] applied surface-to-surface penalty contact enforcement between different surfaces to solve the problem. Nevertheless, this method is inapplicable for patients with OA due to intensity tuning and boundary discontinuities in defected cartilage areas. However, conventional algorithms have been used in a number of studies for automated segmentation of symptomatic knee OA with defected cartilage surfaces [89, 90, 91].

Most of the conventional segmentation methods highlighted the fact that there are still improvements to be made to reach clinically acceptable results despite the simple procedure of these algorithms and thereof computationally efficient operations. This is mainly due to their dependence on the threshold (global or spatial varying) value and post-processing [54]. Finding a proper threshold value or the use of single threshold (i.e. hard thresholding) can be the major reason of segmentation error due to the random noise and artefacts, intensity inhomogeneities, and partial volume effect (PVE) [54]. All these problems make the articular cartilage segmentation in knee MRIs of osteoarthritic patients a challenging problem. However, there are some research efforts to combine simple thresholding methods with other methods to develop more sophisticated segmentation algorithms. In 2010, Dodin et al. [89] reported a slightly more advanced two-level (bright and dark tissue intensity levels) spatial gradient projection thresholding-based method to automatically segment cartilaginous soft tissues from bony and other non-interest tissues. The proposed algorithm used Otsu thresholding algorithm [92] to compute the separation threshold based on a mixture of two Gaussian distribution models defined for intensity level and texture homogeneity of bright and dark tissues. Dodin et al. [89] tested their proposed method namely texture analysis with osteoarthritic knee MRI and validated the stability

of the segmentation method in two time-points. They demonstrated that their texture analysis method can automatically identify the pathological changes in patients with OA by separating the cartilage tissue from synovial fluid [89].

Another successful approach to overcome the issue of uncertain intensity boundaries in segmenting the pathological knee MRIs was proposed by Kubicek et al. [90, 91]. In their *multiregional fuzzy thresholding* approach, a membership function is defined for pixels whose intensity values are within a region (i.e., within the same tissue) [90]. Fuzzy (soft) thresholding method had been previously proposed in [93] in which fuzzy c-means clustering (FCM) [94] is used to obtain the centroids of the clusters. Then, the memberships of each pixel within the region (i.e., clusters in this case) are aggregated to obtain the desired region as a homogeneous area [93].

In order to obtain meaningful segments, domain knowledge should be integrated into the basic algorithms through user interaction and model-driven approaches (such as ACMs and ASMs). A few of them are reviewed in the following section.

3.2. Active contour models

The active contour models (ACMs) or deformable models are widely used in medical image segmentation [95], as well as articular cartilage segmentation and quantification [96]. ACMs are deformable curves used to depict the outline of objects based on the intensity gradient information [41]. ACMs allow utilising image data, shape, appearance, and spatial information of anatomical structures [95]. As a first step in the ACM, the localisation of the cartilage surface starts with a drawn closed curve in the vicinity of articular cartilage region. Next, the curve deformation procedure starts warping based on energy function and this process continues deforming until the deformable model converges to the final segmentation result [47, 96].

ACMs can be represented in either explicit (parametric) or implicit (geometric) forms [41, 97, 98]. Parametric ACM (also called snakes) was first proposed by Kass et al. [99]. In ACM, the segmentation is defined as an optimisation problem where the energy function \mathbb{E} over a deformable curve $r(s)$ at point s , as shown below:

$$\mathbb{E} = \oint_{r(s)} (\alpha \mathbb{E}_{Int}r(s) + \beta \mathbb{E}_{Ext}r(s)) ds \quad (1)$$

In the formulation proposed by Kass et al. [99], \mathbb{E} has two energy minimisation terms, $\mathbb{E}_{Int}r(s)$ and $\mathbb{E}_{Ext}r(s)$. Minimising \mathbb{E}_{Int} permits elasticity and stiffness of the curve or surface throughout deformation (commonly known as internal energy), while \mathbb{E}_{Ext} enforces external constraints to control the curve or surface either towards or away from the image features of adjacent regions (external energy) [47, 95, 97]. α and β are weight constants and balance the elasticity (i.e., internal term) against stiffness imposed by external term [41].

Minimising internal energy leads to contour serving as a spline curve [97]. B-spline snakes [45, 77, 83, 100] and Bezier splines [81, 101, 102, 103] are two commonly used ACMs to segment articular cartilage. Stammberger et al. [45] used B-spline snakes for cartilage segmentation. The segmentation process starts with user initialisation by placing control points along the cartilage boundary using B-spline snake techniques. The gradient strength of the image imposes the force on the contour, and the deformation process continues until a valid result is achieved. A weight factor was assigned to the curve points using the gradient vector projection obtained from Prewitt convolution kernel [104]. The overall average root-mean-square error (RMSE) of cartilage thickness measurement of 0.31 mm was reported in [105], which would require less time and it can be sometimes better than manual segmentation. A summary of ACM-based studies is presented in Table 4.

The main problem with most ACMs is their sensitivity to initialisation and the need for user interaction. In order to address the initialisation problem, two strategies have been applied: (1) using segmentation results of the current slice to initialise the next slice; (2) registering inter- and intra-subjects that correspond to anatomical points.

An alternative method to minimise user interaction is based on the registration of point-to-point correspondence between adjacent slices in 2D space or between baseline and follow-up scans [106, 107, 27]. Carballido-Gamio et al. [101] used elastic registration based on radial basis functions (RBFs) [108] to register corresponding anatomic points between two structures (shape context) of inter-subject and affine registration (i.e., iterative closest point (ICP) algorithm [109]) for intra-subject registration. The reproducibility of cartilage thickness for intra-subject was 2.41% between baseline and follow-up scans.

Kauffmann et al. [110] used local coordinate system (LCS) to map the corresponding cartilage geometry over time. The highest reproducibility of cartilage volume was attained for tibia surface (coefficient of variation (CV) = 0.11%),

while femur exhibited inferior reproducibility ($CV = 0.13\%$) [110]. This interactive cartilage assessment tool is called *ArthroVision*. LCS generates a standard view of cartilage geometry, where the location of each point on inner-boundary (i.e., BCI contour lines) is mapped to 3D simple geometric models (a cylinder for the femur and a plane for tibia) as offset. Figure 8 illustrates the geometry mapping, as defined by *ArthroVision* [111].

Table 4: Summary of ACM methods. Acronyms are from left to right (in order of appearance). Method: semi-automatic (SA), fully automatic (FA). Biomarkers: cartilage thickness (ThC), volume of the cartilage (VC), total area of the subchondral bone (tAB). Dataset: number (#) of subjects (healthy asymptomatic (h) / patients having symptomatic knees (p)). Metrics: coefficient of variation (CV), root mean square error (RMSE). These measurements can be calculated on the knee compartments: patellar cartilage (cPT), medial tibial cartilage (cMT), lateral tibial cartilage (cLT), total femoral cartilage (cF), total tibial cartilage (cT).

Method (SA/FA)	MR pulse sequence	Biomarker	Dataset # subjects (h/p)	Metrics
Cubic B-spline [45] (SA)	FS 3D-FLASH	ThC, VC	in-house 15h	$CV_{cPT} = 4.1 - 5.9\%$ $CV_{cT} = 6.1 - 13.6\%$
Weighted cubic B-spline [105] (SA)	FS 3D-SPGR	ThC, tAB	in-house 6 cadaveric knees	RMSE = 0.31 mm
Bezier spline & shape context & point matching [81, 101] (SA)	WE 3D-SPGR 3D-FSE	ThC	in-house 6h	CV = 2.41%
ACM & geometric mapping (<i>ArthroVision</i>) [110, 111] (SA)	FS 3D-SPGR	ThC, VC	in-house 20h	$CV_{cF} = 0.13\%$ $CV_{cT} = 0.11\%$
ACM [112] (SA)	WE 3D-DESS	ThC, VC	OAI 7h, 8p	$RMSE_{ThC} = 1.9 - 5.2\%$ $RMSE_{VC} = 2.5 - 8.6\%$
ACM [113, 114] (SA)	FS 3D-SPGR	ThC, VC	OAI 3h, 9p	$RMSE_{ThC} = 0.8 - 1.5\%$ $RMSE_{VC} = 0.9 - 1.2\%$ $RMSE_{tAB} = 0.6 - 2.7\%$
dGVF snakes [115] (SA)	WE 3D-FLASH	ThC	in-house 3 cadaveric knees	$RMSE_{ThC} = 1.34 - 2.97\%$

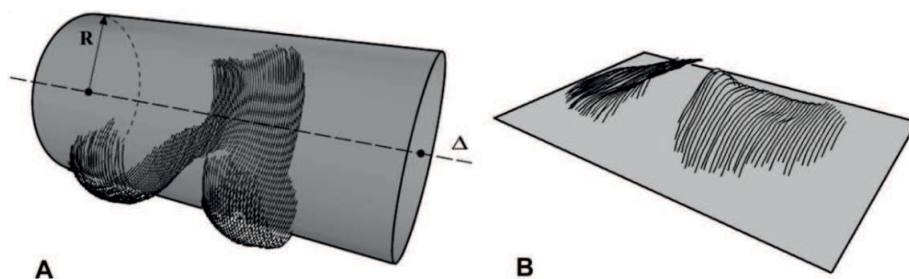


Figure 8: LCS is defined and fitted to the 3D BCI contours manually, as delineated by the user using ACM-based *ArthroVision* software tool. (A) a cylinder for the femur, and (B) a plane for tibia. Copyright 2003 by the Osteoarthritis and Cartilage. Reprinted with permission from [111].

Duryea et al. [112, 113, 114] managed to minimise user interaction in ACM-based method by starting the seg-

mentation from the centre slice of consecutive MRI since the cartilage shape is more consistent near the medial compartment of the cartilage. This method enhanced reproducibility of cartilage thickness (ThC), volume (VC), and subchondral bone surface area (tAB) in paired dataset after manual registration of scans series [114] (see Table 4). In 2011, Iranpour-Boroujeni et al. [116] improved the level automation of ArthroVision by placing two-point landmarks at the outer-most “tips” of the cartilage compartment in each slice to constrain the segmentation region (see Figure 9 and Figure 10).

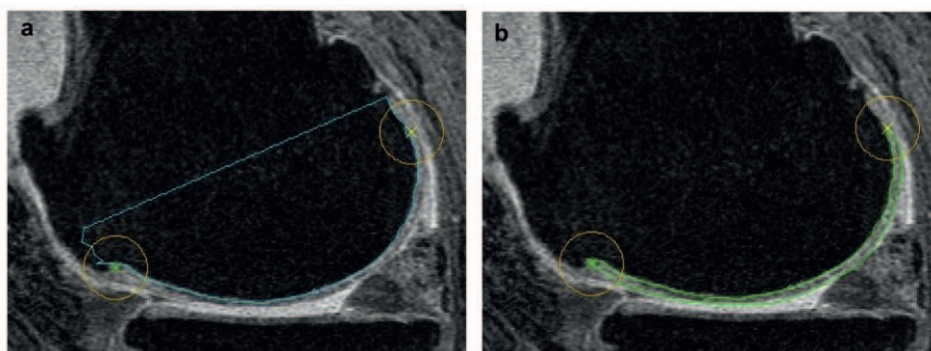


Figure 9: Landmark placing in ArthroVision to minimise user interaction by (a) placing two points at end-points of cartilage soft tissue, near the BCI, (b) segmenting the cartilage region. Copyright 2011 by the Osteoarthritis and Cartilage. Reprinted with permission from [116].

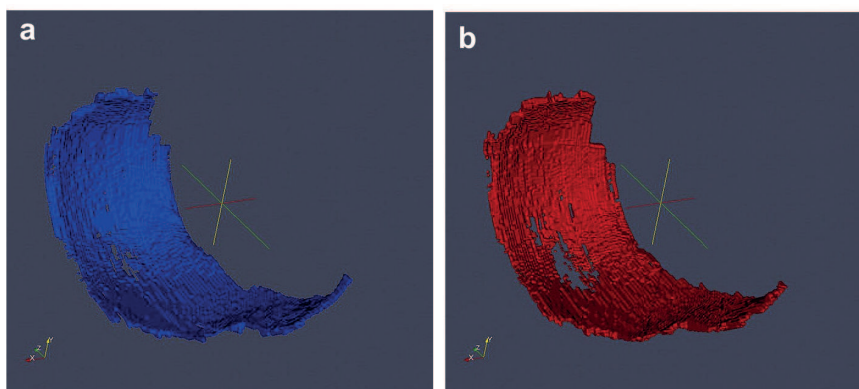


Figure 10: Three-dimensional rendering of a patient having symptomatic knee OA segmented using ACM-based ArthroVision software tool. Articular cartilage visualisation represents the location of cartilage thinning at (a) baseline, and (b) 24 months follow-up scan of the same patient. Copyright 2011 by the Osteoarthritis and Cartilage. Reprinted and adapted with permission from [116].

Although parametric ACM is robust to noise as it constrains the extracted boundaries to be smooth; the deformation process may stop abruptly. This can be due to the noise where local minimum energy is found, hence leading the snake to converge to an incorrect boundary. Snakes suffer from poor convergence to boundaries with large curvatures [54]. In order to address these shortcomings, Xu and Prince [117] introduced gradient vector flow (GVF) snakes. GVF refers to additional external force based on the edge map and overcomes the following two drawbacks in snakes:

- Leakage of energy function at weak boundaries
- Difficulties in the contour evolution at boundaries with concavities

In the case of knee articular cartilage segmentation, a modified version of GVF snakes was proposed to improve the performance of segmenting articular cartilage surface by embedding gradient directional information into the GVF model, called dGVF [115]. This additional directional edge information makes the snake more stable and converges

to the correct surface. Although it enhances the sensitivity of GVF snakes towards blurred boundaries, its execution time is unacceptably high [97] and user intervention is required to adjust the control points within the region of defect cartilage. Chessboard directional compensated GVF (CDCG) was proposed for knee cartilage segmentation by Chi et al. [97, 98], which is resistant to fuzzy edges and performs three times faster than conventional ACMs. Moreover, the method is insensitive to the initialisation of the snake.

ACMs do not require any training, but they demand initialisation, which must be close to the structure of interest. ACMs achieve poor segmentation in areas with low contrast and imaging artefacts. ACM methods have been mostly validated on healthy subjects, however, ACMs are not able to detect significant changes due to OA defects or variations in thickness and curvature of articular cartilage.

3.3. Active shape and active appearance models

Since the past two decades, statistical shape models (SSMs) seem to be a successful method in medical image segmentation [118]. SSMs are model-based segmentation approaches that seek expected shape and appearance of the structure of interest based on a set of landmarks, which is also known as point distribution model (PDM) [41]. Ideally, a shape model is described based on the geometric representation of the structure of interest parameterised by using training data (i.e., model instances). Later, this parameterised shape model (shape template) is fitted to the data to segment the object from other regions. Typically, SSMs determine the best match of the model to the object in test image [119]. Shape models constrain the segmentation based on the outline and appearance of the structure of interest.

Both ASMs [120] and active appearance models (AAMs) [121], as proposed by Cootes et al., are the two well-known and commonly used SSMs for knee sub-compartment segmentation. This section focuses on shape models by briefly explaining the shape initialisation reported in various studies. A summary of SSM-based approaches for the knee bone and cartilage segmentation is presented in Table 5. The overview of statistical shape approaches, including shape representation and construction, is based on those reported in [118] and [119].

Based on the seminal work by Cootes and Taylor [119, 120]; the shape analysis pipeline can be divided into two phases: *training* phase and *segmentation* phase. The process of creating (training phase) and validation (segmentation phase) is described in detail in [122].

In the training phase, *landmarking* is the first stage that must be performed by an experienced radiologist. Landmarking is the simplest method that represents the shape with a set of points distributed across the surface. Then, at *surface mesh extraction* stage, a surface mesh is created (by, e.g., Marching Cubes algorithm [123]) from the manual segmentation of training samples to keep the connectivity data of point sets. Then, in order to compare equivalent points on varied shapes in the training set, the shapes must be aligned with respect to a set of axes in the *surface alignment* step. Procrustes alignment (PA), as described in [124], is the most popular method for the surface alignment that reduces the mean squared distance between equivalent points (i.e., shapes). At the stage of *shape correspondence*, a dense point correspondence is established between all training set shapes. The dense correspondence offers anatomically consistent coordinates between the equivalent points on the structure of interest across the population. Upon alignment and point correspondence establishment of each training surface, principal component analysis (PCA) [125] yields a linear model (*at 3D shape model construction* stage) to capture intrinsic shape variations. A shape S can be approximated by a linear shape model constructed from m aligned point coordinates as

$$S(b, T) = T(\bar{x} + \sum_m b_m p_m) \quad (2)$$

where $\bar{x} \in \mathbb{R}^{3m}$ represents the mean shape, $p_m \in \mathbb{R}^{3m}$ are the modes of shape variation (eigen modes), T refers to the affine transformation, b reflects the valid shape parameter, and $b_m \in \mathbb{R}$ in Eq. (2) reflects the shape weights. Figure 11 displays the primary mode of variations for patella, tibia, and femur bones.

The first step in the segmentation phase is to locate an SSM on the test image data, wherein a local or global search algorithm is required to estimate the initial pose of the model. *Shape initialisation* can be performed either manually or automatically. Multi-resolution search is a coarse-to-fine search strategy [127], in which a set of grey-levels are built for each level. Once the search ends at the coarse resolution level, the search switches to the next resolution level. This does not only speeds up search time but also enhances the robustness and quality-of-fit measure. In 1996, Solloway et al. [46, 128] proposed a 2D ASM framework to segment femur bone (bF) and total femoral cartilage (cF) boundary that followed the seminal works by Cootes and Taylor [120, 119]. They estimated the position of cF by

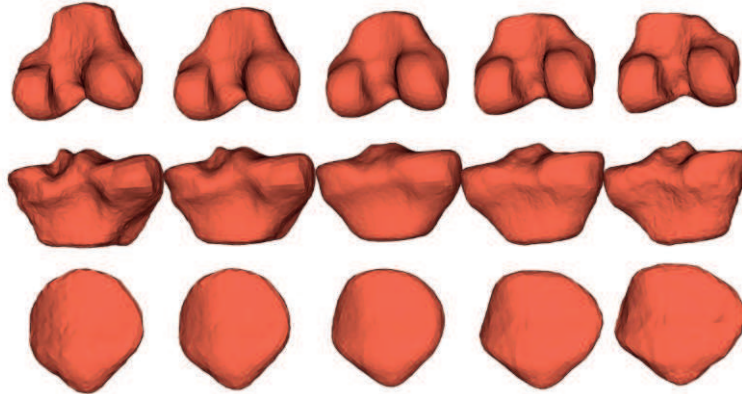


Figure 11: The primary principal mode of variation (eigenmode) of an SSM for the femur (top row), tibia (middle row), and patella (bottom row) bones. Bone models varied by $\pm \sqrt{3}$ standard deviations. Copyright 2005 by the Springer Nature. Reprinted with permission from [126].

assessing a small normalised gradient patch (NG-profile) around each landmark [128]. During the search, the fit of a multi-resolution grey-level profile at the landmark points is assessed by determining the Mahalanobis (Mah) distance between the patch and multi-resolution models. González and Escalante-Ramírez evaluated different methods to segment cF, including the combinations of ASM with local binary pattern (LBP) (ASM-LBP) descriptors [129], and ASM with contrast-enhanced images using image fusion (ASM-Fusion) [130] to gain a new appearance model for ASM to initialise a search.

After the initialisation step, a surface mesh (i.e., shape instance) is propagated to the initial segmentation, and the shape instance is registered to the mean shape using affine similarity transformation. Then, a shape parameter vector is assigned to the shape and results in a deformed and estimated shape.

Fripp et al. [131] proposed to re-parameterise the surface coordinates onto inverse mapping of the landmark with barycentric coordinates obtained via intersection algorithm [132] for automatic initialisation of 3D ASM. This method was later extended to segment the bone [133] and cartilage [134] within the whole joint. They automatically initialised 3D ASM using affine registration [135]. This method significantly improved the speed of local search and the accuracy of the final segmentation. Their method reported DSC of 87%, 87%, and 85.5% for patellar cartilage (cPT), cF, and total tibial cartilage (cT), respectively (see Table 5). They claimed 96% of DSC for knee bone segmentation [133]. Seim et al. [136] extended the Generalised Hough transform (GHT) to incorporate the pose initialisation of SSMs. Nevertheless, the necessary look-up table (i.e., accumulator array) is unfeasible for 3D space. Hence, Seim et al. [136] applied a more constrained transformation by limiting the range of scale and rotation.

Table 5: Knee cartilage segmentation tasks solved with statistical shape models. Acronyms are from left to right (in order of appearance). Method: semi-automatic (SA), fully automatic (FA). Biomarkers: cartilage thickness (ThC). Dataset: number (#) of subjects (healthy asymptomatic (h) / patients having symptomatic knees (p)). Metrics: coefficient of variation (CV), Mahalanobis distance (Mah), specificity (SP), sensitivity (SN), Dice similarity coefficient (DSC), volumetric overlap error (VOE), root-mean-square symmetric surface distance (RMSD), Hausdorff distance (HD). These metrics can be calculated on the knee compartments: total femoral cartilage (cF), femur bone (bF), patellar cartilage (cPT), patella bone (bPT), tibia bone (bT), total tibial cartilage (cT).

Method (SA/FA)	Initialisation (search algorithm)	Correspondences	MR pulse sequence	Dataset # subjects (h/p)	Metrics
2D ASM [128] (FA)	multiresolution searching (NG-profile (Mah))	point matching	FS 3D-SPGR	in-house train:(12h,16p) test: 6h	$CV_{ThC} = 2.8\%$
3D ASM [131] (FA)	quasi-uniformly sampling	ICP & simplex-PF	FS 3D-SPGR	in-house 12h (leave-one-out)	$SN_{cPT} = 71.15\%$ $SP_{cPT} = 99.24\%$ $DSC_{cPT} = 44.37\%$

Continued...

Table 5 Continued. . .

Method (SA/FA)	Initialisation (search algorithm)	Correspondences	MR pulse sequence	Dataset # subjects (h/p)	Metrics
3D ASM [133] (FA)	affine registration	MDL optimization	FS 3D-SPGR	in-house 20h (leave-one-out)	$DSC_{bPT} = 89\%$ $DSC_{bF} = 96\%$ $DSC_{bT} = 96\%$
3D ASM [134] (FA)	affine registration	MDL optimization	FS 3D-SPGR	in-house 20h (leave-one-out)	$DSC_{cPT} = 87\%$ $DSC_{cF} = 87\%$ $DSC_{cT} = 85.5\%$
3D ASM [136] (FA)	GHT	mesh-to-mesh	Many (T1, T2, etc.)	SKI10 train:60 (h,p) test:40 (h,p)	$VOE_{cF} = 34.0\%$ $VOE_{cT} = 29.2\%$ $RMSD_{bF} = 1.54$ mm $RMSD_{bT} = 1.24$ mm
AAM [53] (FA)	multiresolution exhaustive search & registration	MDL optimization	Many (T1, T2, etc.)	SKI10 train:60 (h,p) test:40 (h,p)	$VOE_{cF} = 36.3\%$ $VOE_{cT} = 34.6\%$ $RMSD_{bF} = 1.49$ mm $RMSD_{bT} = 1.21$ mm
ASM-LBP [129] (FA)	NG-profile (Mah)	point matching	T2	in-house N/A	$HD = 3.0709$ mm $DSC = 81.32\%$

A simple class of correspondence detection is point-matching to seek a set of optimal transformation parameters (translation, scaling, and rotation). In 2D models, this is an effective strategy to determine a good fit that calculates a mean point-to-point error. The ICP is a popular surface matching algorithm to identify the correspondence between two surface meshes, which is also known as mesh-to-mesh registration [118]. Fripp et al. [131] utilised ICP and followed by parameter fitting (PF) via Nelder-Mead simplex algorithm [137] (simplex-PF) to match spatially closest points. However, the drawback of ICP is that it leads to non-homoeomorphic mapping and flipping triangles in the mesh. In [133, 134], correspondence was formulated as an issue of optimisation by utilising minimum description length (MDL) [138], as previously employed by Williams et al. [139, 140] for knee bone segmentation. MDL is a group-wise (population-based) correspondence approach that minimises an objective function by assessing the re-parameterisation of landmarks position. The method seems promising for medical imaging as it delivers good correspondence of all samples at the same time [118]. Vincent et al. [53] used AAMs and MDL for knee joint segmentation and examined the framework on SKI10 dataset in MICCAI2010 contest [51]. Their approach had a lower root-mean-square symmetric surface distance (RMSD) of 1.49 mm and 1.21 mm for femur and tibia bones respectively, when compared to the other contestants [136]. However, [136] with a volume overlap error (VOE) of 34.0% and 29.2% for cF and cT respectively, performed slightly better than [53] (see Table 5).

The segmentation frameworks based on SSMs have to be initialised, either manually or automatically. Image registration is a typical strategy for initialisation [141]. Fripp et al. [133, 141] analysed the inclusion of priori data and the key role of spatial relationship information in automatic initialisation and segmentation of SSMs. It must be emphasised that the probability of expected cartilage thickness and BCI extraction play a crucial role in model initialisation and robustness of segmentation. As opposed to other methods mentioned above, ASMs and AAMs need to train a model in order to capture the variation of appearance and shape at segmentation.

3.4. Graph-based methods

The graph-based segmentation techniques refer to a wide family of algorithms, in which pixels or voxels in an image sequence and the neighbourhood relations among them can be conceptualised as a weighted undirected graph. Graph cuts (Gcuts) was proposed in 2001 by Boykov and Jolly [142]. Let $G = (V, E)$ be a graph where V refers to pixels as a set of vertices, and E is the edge between two vertices connected by that edge. The edge, E , for example, between v_A and v_B nodes, has a corresponding weight $w(v_A, v_B)$ that reflects a measure of similarity between the nodes.

Similarity criterion is computed from the intensity, colour, spatial distribution, texture, gradient, or any other attribute between two vertices [41]. An image is partitioned into a set of uniform and homogeneous regions (i.e. subgraphs); A_i and A_j , wherein $A_i \cup A_j = G$ and $A_i \cap A_j = \phi$ by removing the edges that connect these two subgraphs. The degree of dissimilarity between two subgraphs A_i and A_j can be computed using Gcuts. The Gcuts methods generate two or more disjoint subgraphs, in order to maximise similarity (i.e., weights) within the subgraphs and to minimise dissimilarity across various subgraphs. The sum of weights of discarded edges can be computed as:

$$cut(A_i, A_j) = \sum_{v \in A_i, v \in A_j} w(v_{A_i}, v_{A_j}) \quad (3)$$

where v_{A_i} and v_{A_j} are two vertices in two disjoint subgraphs, and the total weights of edges are called as a *cut*. Minimising this *cut* makes subgraphs dissimilar. Nonetheless, cutting a graph into subgraphs in an optimal manner is not straightforward. Thus, a possible solution for this problem is to minimise the cut in Eq. (3) via optimisation methods [41]. A comprehensive review on graph-based segmentation method is provided in [143, 144].

Gcuts was applied for image segmentation by Wu and Leahy [145], who formulated a cost function, namely minimal cut, in the form of Eq. (3). Gcuts methods for image segmentation can be used either interactively or automatically. Interactive Gcuts is employed extensively for biomedical image segmentation, in which prior knowledge from a user is embedded into image local and boundary attributes.

Image segmentation using Gcuts was formulated into energy minimisation task on an MRF framework to minimise the cost function via dual terms: regional (R_p) and boundary terms ($B_{p,q}$) [142], as follows:

$$E(f_p) = \sum_{p \in P} R_p(f_p) + \lambda \sum_{(p,q) \in N} B_{p,q}(f_p, f_q) \quad (4)$$

where a label f_p is assigned to a voxel p in P , $R_p(\cdot) = -\ln(P(I_p|k))$ represents conditional probability of intensity value I_p given the class $k \in \{0, 1\}$ (either background or cartilage). The smoothness term, $B_{p,q}(\cdot)$, is calculated for N -D neighbourhood system to measure the interaction potential between neighbouring nodes (i.e., p and q). The coefficient λ specifies the importance of smoothness term versus regional term. The term $B_{p,q}(\cdot)$ is calculated by using the following function [146]:

$$B_{p,q}(f_p, f_q) = \exp\left(-\frac{(I_p - I_q)^2}{2\sigma^2}\right) \frac{1}{\|p - q\|} \quad (5)$$

One prominent optimisation strategy for energy function in interactive Gcut is s/t Gcuts [146]. The user starts to loosely place the seed points to impose ‘‘hard constraints’’ over the structure of interest and then modifies the segmentation result by augmenting extra user-specified ‘‘soft constraints’’ near the object boundary. Two types of seeds are manually positioned. One type of seeds is used to specify cartilage, while the other is placed over adjacent non-cartilage background tissues (bone, joint fluid, menisci, etc.). Some authors have used s/t Gcut methods for cartilage segmentation [48, 147, 148]. Figure 12 shows segmentation results using this method. Shim et al. [148] compared the mean processing time and the mean volume overlap between Gcut and manual segmentation on OAI dataset with 10 subjects. The Gcut technique reported 94.3% overall volume overlap compared to 87.8% for manual segmentation (see Table 6).

Shape and appearance priors have been incorporated in Gcuts to ensure that the segmentation procedure to follow the shape prior. Lee et al. [149, 150, 151] proposed a method based on Gcuts for bone and cartilage segmentation. In this framework, the shape prior was integrated into all potentials to control their behaviour. Based on the constrained branch-and-mincut tree search [152], a lower bound of energy for a given set of shape priors was computed to reduce the computational time inherent in conventional s/t Gcuts on 3D space. The characteristic of this framework is to use mean shape constructed from the bone segmentation masks to gain coarse segmentation. From the bone segmentation, Hamming distance of the current voxel corresponds to a specific shape template is constructed to align the input bone [149]. Next, anchor points are extracted from the distance transformation map to extract local patches around BCI for cartilage segmentation. They showed that combining shape and appearance prior potential in both regional and boundary terms could enhance the robustness of segmentation [149]. This method compared to the interactive Gcut (DSC = 94.3%) has reported DSC of above 95% for the three main knee bones. Knee joint segmentation errors mostly occur in patients with a late-stage osteoarthritis grade, which is characterised with large osteophytes and the presence of denuded cartilage surface. As illustrated in Figure 13 the method proposed in [151] is robust in detecting

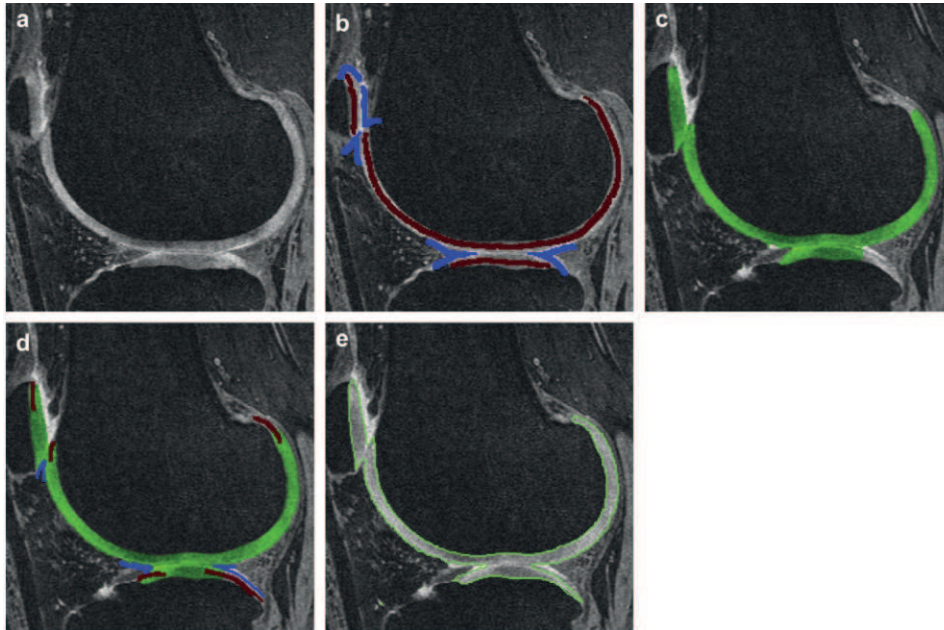


Figure 12: Cartilage interactive segmentation using s/t Gcut method: (a) original image, (b) an expert positioned seed points over cartilage (red lines) and background surrounding tissues (blue lines), (c) Gcut segmentation results, (d) revision of seeds, and (e) final cartilage segmentation result. Copyright 2009 by the Osteoarthritis and Cartilage. Reprinted with permission from [147].

the morphological defects in the articular cartilage (Figure 13 (C,D)) and other knee structure abnormalities such as osteophytes (Figure 13 (A,B)).

Table 6: Summary of graph-based methods. Acronyms are from left to right (in order of appearance). Method: semi-automatic (SA), fully automatic (FA). Dataset: number (#) of subjects (healthy asymptomatic (h) / patients having symptomatic knees (p)). Metrics: Dice similarity coefficient (DSC), volumetric overlap error (VOE), root-mean-square symmetric surface distance (RMSD), surface positioning error (Err). These metrics can be calculated on the knee compartments: patellar cartilage (cPT), total femoral cartilage (cF), total tibial cartilage (cT), patella bone (bPT), femur bone (bF), tibia bone (bT), medial femoral cartilage (cMF), lateral femoral cartilage (cLF), medial tibial cartilage (cMT), lateral tibial cartilage (cLT).

Method (SA/FA)	Optimization method	MR pulse sequence	Dataset # subjects (h/p)	Metrics
Interactive Gcut [148] (SA)	min-cut/max-flow	3D-DESS	OAI 1h,9p	$DSC_{overall} = 94.3\%$
Combined shape and appearance potentials [151] (FA)	Constrained branch-and-mincut	3D-DESS	OAI train:10 (h,p) test:7 (h,p)	$DSC_{bPT} = 95.4\%$ $DSC_{bF} = 95.2\%$ $DSC_{bT} = 96.4\%$
[150] (FA)		Many (T1, T2, etc.)	SKI10 train:60 (h,p) test:40 (h,p)	$VOE_{cF} = 30.6\%$ $VOE_{cT} = 34.0\%$ $RMSD_{bF} = 2.56 \text{ mm}$ $RMSD_{bT} = 1.40 \text{ mm}$

Continued...

Table 6 Continued. . .

Method (SA/FA)	Optimization method	MR pulse sequence	Dataset # subjects (h/p)	Metrics
Gcuts on pre-segmented images (LOGISMOS) (gradient-based cost functions) [153] (FA)	min-cut/max-flow	WE 3D-DESS	OAI train:34 (h,p) test:60 (h,p)	$DSC_{cPT} = 80\%$ $DSC_{cF} = 84\%$ $DSC_{cT} = 80\%$
LOGISMOS & JEI post-processing (learning-based cost function) [154] (FA)	min-cut/max-flow	3D-DESS	OAI train:28 (h,p) test:53 (h,p)	$Err_{bF} = 0.03$ mm $Err_{bT} = 0.10$ mm
[155] (FA)		3D-DESS	OAI train:34 (h,p) test:108 (h,p)	$Err_{cMF} = -0.04$ mm $Err_{cLF} = -0.26$ mm $Err_{cMT} = -0.15$ mm $Err_{cLT} = -0.03$ mm

In 2010, Yin et al. [153] proposed a strategy called LOGISMOS (layered optimal graph image segmentation of multiple objects and surfaces) by integrating Gcuts into pre-segmented images. First, coarse pre-segmentation of each object is obtained by applying a deformable shape model or other segmentation technique. Object-specific graphs are generated from the pre-segmented images, while the surfaces are meshed to construct the graph structures for individual objects. The method suggests simultaneous bone and cartilage segmentation, and is composed of three steps:

1. Bone pre-segmentation
2. Mesh generation and optimisation by Gcuts
3. Co-segmentation of knee bone and cartilage surfaces

In the LOGISMOS framework, the optimal surface segmentation has been formulated to seek a net surface with the minimum cost of weights on each node from a directed graph. A multicolumn graph represents the surface mesh between multiple objects. Two spatially-coincident columns of nodes for bone and cartilage are connected with three equidistance arcs: directed inter-column, intra-column, and orthogonal inter-surface arcs. Both inter- and intra-column arcs enforce the stiffness of the output surface and govern the surface smoothness constraints. Nevertheless, orthogonal inter-surface arcs reflect object-interacting surfaces and ensure inter-object constraints.

The cost function of the BCI surface is determined by the first-order derivatives of nodes on the bone surface, while the cost function of cartilage is the weighted combination of first and second-order derivatives. In 2018, Kashyap et al. [154, 155] extended LOGISMOS by integrating a post-processing interaction step known as just-enough interaction (JEI). A hierarchy of random forest (RF) classifiers were used to enhance the location-specific cost functions, where the output probabilities of the second RF (learning-based cost function) serves as the cost function for LOGISMOS. They claimed a significant reduction in signed error of bone surface positioning for femur bone (0.03 mm), when compared to tibia bone [154]. The learning-based cost function on all cartilage compartments had been assessed [155]. The study reported significant reduction in both signed and unsigned cartilage surface positioning errors (p-value $\ll 0.001$), except on the medial tibial cartilage (cMT) (p-value = 0.193). They compared the results between gradient costs and learning costs and demonstrated a significant improvement in the segmentation results obtained by using learning costs both quantitatively and qualitatively. Table 6 presents the signed error of surface positioning for bone [154] and cartilage [155] using learning-based cost function LOGISMOS framework. The learning scheme of LOGISMOS is further discussed in Section 3.6.

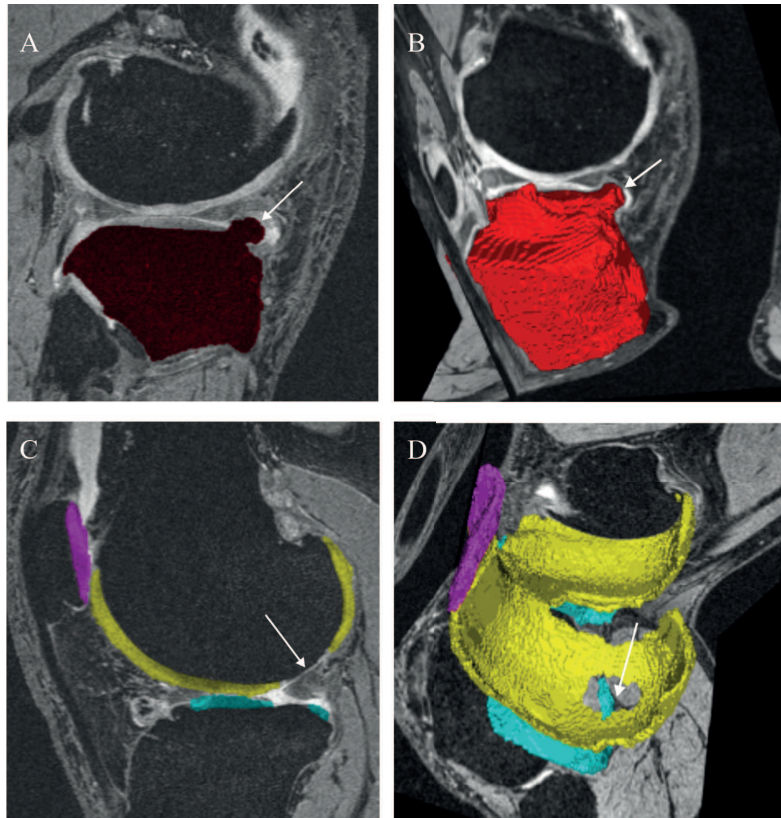


Figure 13: An illustration of the segmentation results obtained by constrained branch-and-min-cut algorithm [151]. The proposed method can robustly segment the MRI data from the patients having last-stage symptomatic OA. (A) Final segmentation result of the tibia bone with osteophyte presence (arrow); (B) 3D rendering of tibia bone; (C) final segmentation results show the cartilage deterioration of an osteoarthritic knee with cartilaginous defect (arrow shows the denuded area); and (D) 3D rendering shows a hole in the degenerated cartilage surface (arrow). Copyright 2011 by the Computer Vision and Image Understanding. Reprinted and adapted with permission from [151].

3.5. Atlas-based methods

In the context of medical imaging, an atlas refers to a reference model composed of labels linked with all structures prior to segmentation. Based on the definition provided by Rohlfing et al. [156], an “atlas” incorporates prior anatomical data (i.e., locations and shapes of an anatomical structure), and distinguishes spatial relationship to other anatomical structures. The atlas-based methods seek to label anatomical structure by mapping the coordinates of a given image to anatomical pre-constructed atlases [156]. This process is known as registration, where the label of each image voxel is assigned by looking up the label of the structure at the corresponding location in the atlas. This labelling process refers to an image that is co-registered to an atlas known as atlas-based segmentation or registration-based segmentation.

Various atlas-based segmentation methods have been used to select a possible atlas and categorised based on the type, number, and fixed/variable assignment of atlases [156]. Typically, these methods are composed of three steps: atlas construction, registering the atlas template to target image, and atlas propagation (atlas warping). Shan et al. [157] classified atlas-based segmentation strategies into three classes, as listed below:

1. *Single atlas*: a random individual segmented image with the best quality and fewer artefacts is selected as an atlas. Next, all the remaining raw images are non-rigidly registered to the atlas (reference) image.
2. *Average shape atlas (probabilistic atlas)*: an average and normalised atlas is generated from the population images, and then, the images are registered to the average atlas.
3. *Multiple atlas*: a set of multiple reference images is constructed, and a given raw image is independently registered to each atlas.

In the case of knee joint segmentation, this method has gained popularity in the recent decade [157, 158]. For example, six atlases were constructed from healthy patients by manually tracing their bones and cartilages [158]. All atlases were registered to the input image by optimising normalised mutual information (NMI) similarity measure. Upon completing the registration process, a fuzzy voting algorithm is used to combine the outputs of all segmentations into a single label per voxel. Tamez-Peña et al. [158] reported high reproducibility and an improved DSC (88%) of femoral cartilage, in comparison to those reported in [69, 141] (see Table 7). Similarly, Shan et al. [157, 159, 160] extended the work of [158] by using multiple atlases for bone segmentation.

Since articular cartilage has varying tissue properties, constructing an atlas can be a challenging task, as it demands an accurate approach to segment the thin cartilage area. One major issue in cartilage segmentation refers to overlapping the segmented compartments of femoral and tibial cartilage. This decreases the accuracy of the segmentation method.

The bone-cartilage atlases are built for femur and tibia bones first, and then, either multi-atlas or average shape atlas is applied for cartilage segmentation in order to address the issue of overlapping cartilage compartments [157, 159, 160]. Multi-class segmentation and three-label segmentation have been proposed to segment femoral and tibial cartilage simultaneously, and have been successfully performed for bone segmentation [159, 160]. All these work [157, 159, 160] used affine registration and B-spline registration based on mutual information for label propagation on the input image. The propagation of average shape transformation is performed iteratively for each image.

One limitation of label propagation is the fact that the propagated label cannot be generalised, which hinders the accuracy. To overcome this drawback, label fusion techniques have been proposed. Majority voting, locally-weighted, and non-local patch-based label fusion methods have been applied as alternative approaches to the average shape atlas for cartilage segmentation [157]. Shan et al. [157] computed the average of all atlases registered for cartilage segmentation to compute the label by using the majority voting label fusion technique [156]. The weighted sum of the classification is retrieved from the atlases, in which higher weight is given to atlases that manage to determine the maximum likelihood of cartilage. This is also known as weighted convolution. Locally-weighted label fusion technique has displayed better segmentation accuracy in SKI10 dataset (see Table 7). This method has been ranked fifth amongst the top 8 methods in SKI10 challenging dataset [157].

Table 7: Summary of atlas-based methods. Acronyms are from left to right (in order of appearance). Method: semi-automatic (SA), fully automatic (FA). Dataset: number (#) of subjects (healthy asymptomatic (h) / patients having symptomatic knees (p)). Metrics: Dice similarity coefficient (DSC). These metrics can be calculated on the knee compartments: patella bone (bPT), femur bone (bF), tibia bone (bT), patellar cartilage (cPT), total femoral cartilage (cF), total tibial cartilage (cT).

Method (SA/FA)	Registration algorithm	MR pulse sequence	Dataset # subjects (h/p)	Metrics
Multiple atlas [158] (FA)	affine registration & B-spline registration	WE 3D-DESS	OAI 48 scans (12 subjects (6h,6p): scan-rescan;2 time-points)	$DSC_{cF} = 88\%$ $DSC_{cT} = 84\%$
Average shape (probabilistic) atlas [161] (FA)	affine registration	Many (T1, T2, etc.)	SKI10 atlas creation: 15 (h,p) test:40 (h,p)	$DSC_{cF} = 78.2\%$ $DSC_{cT} = 82.6\%$
Multiple atlas & locally-weighted label fusion [157] (FA)	affine registration & B-spline registration	Many (T1, T2, etc.)	SKI10 atlas creation: 15 (h,p) test:40 (h,p)	$DSC_{cF} = 85.6\%$ $DSC_{cT} = 85.9\%$
Multiple atlas & locally-weighted label fusion & local structure analysis [162, 163] (FA)	affine registration & B-spline registration	Many (T1, T2, etc.)	SKI10 train:60 (h,p) test:40 (h,p)	$DSC_{cF} = 71.7\%$ $DSC_{cT} = 72.4\%$

As for the fusion strategy, Lee et al. [162, 163] used locally-weighted vote (LWV) around each voxel from a test image (registered with an atlas), and the label with maximum convoluted value was selected as the target label. Next, Gcut was embedded to correct any abnormality. At registration, n -best matched atlases are ranked based on mutual information similarity measure. Then, the local structure analysis was integrated into LWV to obtain the probability of a voxel as cartilage, mainly due to the thin structure of cartilage and intensity variation [162].

Atlas-based methods bring out the robustness to the segmentation strategy. Table 7 shows that multiple atlases are the most widely-used method for knee bone and cartilage segmentation. Nonetheless, building multiple atlases and registering them to the whole population of test data incur a computational burden on the model. This approach, hence, can serve as initialisation or as a prior for other methods [133].

3.6. Learning-based methods

In the last decade, a new generation of frameworks has been developed to address challenges related to knee joint segmentation by using learning-based methods or machine learning strategies. The goal of the learning-based method is to learn the features of each pixel I_i from data and to assign a segmentation label, ($l_i \in \{1, 2, \dots, K\}$), to I_i . From the probabilistic stance, such learning-based methods predict a training set of labelled pixels by computing the conditional probability $P(l_i|I_i)$. Studies that apply supervised learning-based methods are discussed in this section. In classical machine learning strategies, supervised learning methods (discriminative models) extract *hand-crafted* features gained from expert knowledge to train a classification model for voxel label prediction.

Deep learning (DL) methods, such as CNNs, have been widely employed in biomedical image segmentation [164]. The CNNs were first introduced by Lecun et al. [165]. The interest in the topic is motivated by the promising results achieved from ImageNet [166]. DL is a method that intelligently learns the features from raw data, which is a purely data-driven procedure for feature representation. The following classifies previous studies based on feature representation; either manually-engineered and hand-crafted or automatically data-driven learned features.

3.6.1. Methods based on hand-crafted features

A supervised method estimates the label of each voxel from hand-crafted features extracted from the image based on an algorithm designed in accordance with expert knowledge. In most studies, the classification is based on hand-crafted features, such as intensity, local image structures, texture, geometric, and semantic context. Table 8 presents further details on commonly used features by various studies for knee cartilage segmentation.

Table 8: Summary of the popular hand-crafted features for knee articular cartilage segmentation.

Category	Features
Intensity	Gradient smoothed intensity at different scales, voxel intensity, mean, variance, skewness, kurtosis
Local	First, second, and third-order gradient derivatives with respect to (x, y, z) , 3 eigenvalues of Hessian matrices, and 3 eigenvalues of structure tensor at different scales ($\sigma = 0.65, 1.1, 2.5$ mm), eigenvectors corresponding to the largest eigenvalues of Hessian and structure tensor matrices
Texture	Haar features (along horizontal, vertical & diagonal direction), Gabor
Geometric	Three-jet, coordinate information of voxels in the image (x, y, z) , 3D Euclidean distance from different knee bone surface (i.e., BCI)
Semantic context & context	Probability maps of each knee compartment obtained from a specific classifier, random shift intensity difference (RSID), random shift probability difference (RSPD)

In 2005, Folkesson et al. [167, 168] pioneered voxel-wise classification, which was introduced using local structure features for knee cartilage segmentation. Multi-class approximate k -nearest neighbour (k -NN)-based classifier was applied to classify each voxel into three classes: tibial and femoral cartilages, or background. They assessed the

performance of the algorithm, beyond accuracy and reproducibility, including computational and memory requirement [169]. The idea is to sample a set of voxels by using a sampling algorithm (e.g. Gaussian sub-sampling) and then to classify it as cartilage or background. If the voxel is classified as cartilage, it will proceed with the classification of adjacent voxels. This process is known as *classification-driven region growing with sample-expand*. The objective is to classify voxels that belong to the structures prior to segmentation. The process attained 99.96% and 81.1%, specificity (SP) and sensitivity (SN), respectively. They also trained two binary *k*NN classifiers for tibial and femoral cartilage using *one-versus-all* approach [167]. The results showed a slight improvement in accuracy when compared to multi-class classification. A summary of the classifications is given in Table 9.

Similarly, Öztürk and Albayrak [170] computed intensity and local features, and trained 4 *one-versus-all k*NN classifiers with varying sub-sampling methods, such as uniform, Gaussian, vicinity-correlated sparse, and vicinity-correlated dense sampling. The method reported the best DSC on OAI dataset after the model was trained with VC sparse sub-sampling. Besides, region detection can minimise computational complexity. For instance, a rectangular structure-wise ROI detection was performed on the registered scans [171].

Another conventional technique is to perform a cascaded learning approach. Prasoon et al. [172, 173] proposed an extended cascaded classification framework originally introduced by [50]. This extended framework is known as a hierarchical classification scheme to segment femoral and tibial cartilage. A *k*NN classifier is performed at the initial stage, while a support vector machine (SVM) classifier is applied at stage two. Their idea derived from the notion that a classifier capable of training massive datasets (such as *k*NN) can be used in the first step to reduce false negatives. Next, voxels classified as background at the first stage were labelled as background and are discarded at the second stage, while all voxels classified as foreground were moved to the second stage of classification. They improved the DSC up to 4.15% and 3.32%, for medial femoral cartilage (cMF) and cMT respectively, which is in line with that reported in [168] based on a similar in-house dataset context.

Learning-based segmentation methods can locate the cartilage region, but a problem arises when they try to segment touching and overlapping areas of the cartilages. They only use local and intensity features without prior spatial knowledge about the surrounding objects. This could increase false positives or false negatives and as a result, it produces ambiguous cartilage boundaries.

Dealing with overlapping cartilage boundaries is still a major challenge in the field of knee structure segmentation. Many schemes that considered multi-modal MRIs [174, 175] and have integrated spatial dependencies [176, 177] have been investigated to separate overlapping and touching structure boundaries. Koo et al. [174, 175] pioneered the use of multi-modal MRIs (five MR sequences) for cartilage segmentation for the first time. Multi-contrast MRIs are used to obtain anatomical information and then to generate the geometrical features of voxels. Since different tissues in the knee, such as bone, cartilage, etc., have various types of morphological properties, the relative appearance in MRI is bound to differ. The feature vector of voxels for each contrast is trained by the SVM-light classifier [178] to separate varying musculoskeletal tissue types [174]. The hyperplane generated from the training process is applied to produce geometrical information of voxels, such as distance between cartilage and bone. A similar approach was used in [176, 177], but they used four MR modalities and combined SVM with a discriminative random field (DRF) to model the spatial dependencies between the neighbouring voxels. The results indicated that joint SVM-DRF improved the DSC up to 88% with none of the compartments achieving below 84% when compared with individual SVM or DRF (see Table 9). Despite the promising results, this algorithm has only been tested on healthy volunteers (Figure 14). Besides, obtaining different MRI sequences may be unfeasible in clinical practices due to expenses, time constraints, and availability.

Apart from the features mentioned above for knee and other medical images, many other hand-crafted features have been designed specifically for knee cartilage segmentation. Wang et al. [179] designed various features to segment cartilage without relying on the BCI extraction step. They developed a learning-based bone segmentation from anatomical correspondence mesh points and calculated the 3D Euclidean distance from the voxels found on the bone boundaries. A subset of “context” features, known as random shift intensity difference (RSID), was extracted to compare the intensity of current voxel with a random offset. They trained an iterative RF (i.e., Hierarchical RFs) method, and the probability maps obtained from the previous stage of the classifier were also used to gain additional contextual information for the second stage of classification. Random shift probability difference (RSPD) is defined as “semantic context” feature and compares the probabilities of voxels with a random shift offset of the current voxel.

In the learning-based approach called LOGISMOS proposed in [155] (see Section 3.4), a hierarchy of RF classifiers was used to provide both global and local information, thus enhancing segmentation accuracy. Neighbourhood

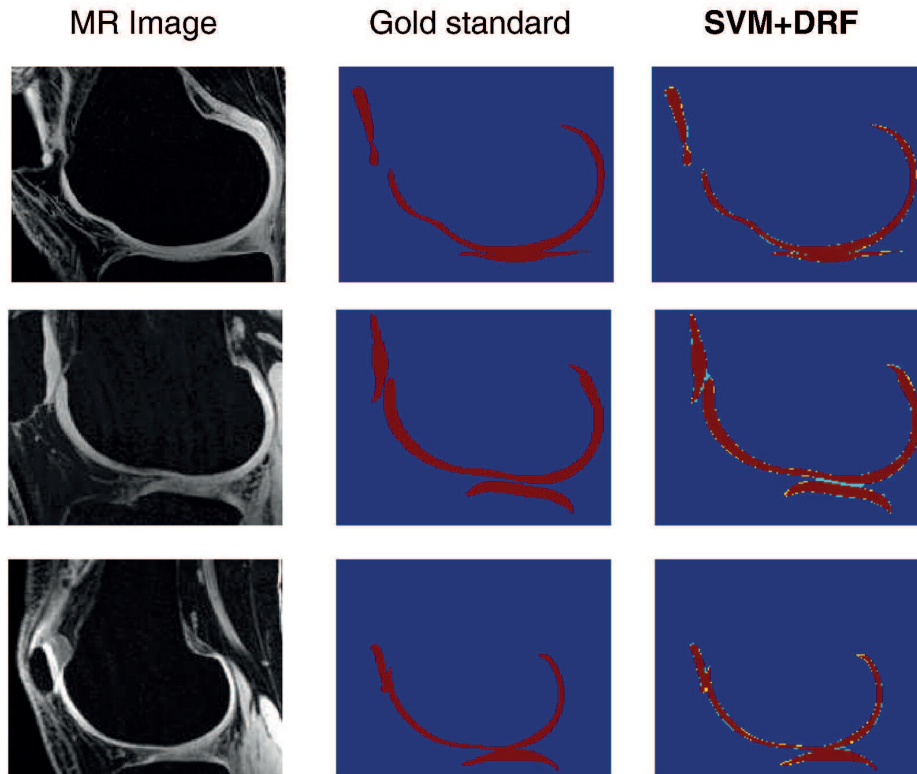


Figure 14: Cartilage automatic segmentation using the joint SVM-DRF proposed by Zhang et al. [177]. The sample 2D MR images from three different healthy volunteers (left column), manual ground-truth segmentation (middle column), and the segmentation results using joint SVM-DRF (right column). Copyright 2013 by the Magnetic Resonance Imaging. Reprinted and adapted with permission from [177].

approximation forests (NAF), and followed by clustered RF classifiers were used to train contextual and structural information. Kashyap et al. [155] employed the probability map output of NAF as context features. Besides contextual and local features, they computed Gabor texture features and Haar features. Their learning-based framework showed high robustness (see Table 6) and a strong correlation (above 98%) with manual segmentation.

Table 9: Summary of learning-based methods. Acronyms are from left to right (in order of appearance). Method: semi-automatic (SA), fully automatic (FA). Dataset: number (#) of subjects (healthy asymptomatic (h) / patients having symptomatic knees (p)). Metrics: Dice similarity coefficient (DSC), specificity (SP), sensitivity (SN), volumetric overlap error (VOE), root-mean-square symmetric surface distance (RMSD). These metrics can be calculated on the knee compartments: medial tibial cartilage (cMT), lateral tibial cartilage (cLT), patellar cartilage (cPT), total femoral cartilage (cF), medial tibial cartilage (cMT), lateral tibial cartilage (cLT), total tibial cartilage (cT), femur bone (bF), tibia bone (bT).

Method (SA/FA)	Features	MR pulse sequence	Dataset # subjects (h/p)	Metrics
Multi-class k NN (Gaussian sampling) [168] (FA)	intensity, local	Turbo 3D-T1	in-house train:25 (h,p) test:114 (h,p)	$DSC_{cMF} = 77\%$ $DSC_{cMT} = 81\%$ SN = 81.1% SP = 99.96%
one-versus-all k NN (vicinity-correlated sparse sampling) [170] (FA)	intensity, local	WE 3D-DESS	OAI train:10 (h,p) test:23 (h,p)	$DSC_{cPT} = 72.6\%$ $DSC_{cF} = 82.6\%$ $DSC_{cMT} = 81.3\%$ $DSC_{cLT} = 84.6\%$

Continued...

Table 9 Continued. . .

Method (SA/FA)	Features	MR pulse sequence	Dataset # subjects (h/p)	Metrics
Multi-atlas context forests (cascaded RF) [180] (FA)	intensity, local texture, context	Many (T1, T2, etc.)	SKI10 train:30 (h,p) test:40 (h,p)	$DSC_{cF} = 81.2\%$ $DSC_{cT} = 80.9\%$ $DSC_{bF} = 97.3\%$ $DSC_{bT} = 97.0\%$
Multi-atlas registration & binary k -NN [171] (FA)	intensity, local	Many (T1, T2, etc.)	SKI10 train:60 (h,p) test:40 (h,p)	$VOE_{cF} = 26.9\%$ $VOE_{cT} = 25.1\%$ $RMSD_{bF} = 1.25$ mm $RMSD_{bT} = 0.91$ mm
Hierarchical framework k NN + SVM [172, 173] (FA)	intensity, local	Turbo 3D-T1	in-house train:25 (h,p) test:114 (h,p)	$DSC_{cMF} = 81.15\%$ $DSC_{cMT} = 84.32\%$
SVM-DRF [177] (FA)	intensity, local, geometric	FS SPGR, FIESTA, and IDEAL GRE (WE & FS).	in-house (multi-modal (4 modalities) MRIs) 11h (leave-one-out)	$DSC_{cPT} = 84.1\%$ $DSC_{cF} = 86.4\%$ $DSC_{cT} = 88\%$
Hierarchical RF + Gcut (post-processing) [179] (FA)	intensity, local, geometric, context, semantic context	WE 3D-DESS	OAI 176 (h,p)	$DSC_{cPT} = 79.16\%$ $DSC_{cF} = 84.96\%$ $DSC_{cT} = 83.74\%$

The idea of registered multiple atlases discussed in Section 3.5 can also be fed into the classifiers. The spatial priors obtained from multiple atlases allow extraction of context features for the classifier. Liu et al. [180] trained varying layers of RFs based on multiple atlases to segment bones and cartilages. Appearances obtained from training images and context features were extracted from the segmentation results of the previous layer of trained RF classifier. The combination of atlas and learning-based technique can improve the accuracy of segmentation [171]. Dam et al. [171] reported 26.9% and 25.1% of VOE for femoral and tibial cartilages on SKI10 dataset, respectively (see Table 9).

Methods that embed geometrical and contextual features into voxel classification framework have attained good segmentation results for various cartilages. In most work, contextual and spatial data come in the form of probability map from the previous classification stage [180, 154, 155] or as a posterior probability cost function fed into Gcut post-processing stage to be maximised [155]. The spatial and appearance data can serve as a shape regularisation post-processing step by using deformable shape models.

Table 9 presents learning-based studies. The patellar cartilage (cPT) is the most difficult structure to segment, with a mean DSC of 79.16% on OAI dataset [179], while the structure that seems to attain better results is the femoral cartilage (cF).

3.6.2. Methods based on deep convolutional neural networks (CNNs)

Many studies have developed algorithms for automated cartilage segmentation that rely primarily on manually engineered features. Nonetheless, there is no general consensus on which specific features are most applicable in segmentation of knee compartments. Thus, DL models, particularly CNNs, have been recently considered as a new method for knee cartilage segmentation [181] and knee OA diagnosis [182]. In comparison to hand-crafted strategies, DL learns features automatically through a hierarchy of multiple layers and numerous parameters [40]. Prasoon et al. [181] reported three trained 2D CNNs, called multi-planar CNNs, for each orthogonal plane of knee MRIs (i.e., sagittal, coronal, and axial). This method displayed superiority of learned features obtained from CNNs (82.49% DSC volume overlap) over hand-crafted features in [168] (see Table 8). A summary of DL-based segmentation methods is given in Table 10.

Despite the success of CNNs, a major problem in biomedical image processing is the lack of large-scale annotated medical images, which has not yet reached in clinical practices. Besides, training CNNs from the scratch using a limited amount of labelled images can easily lead to overfitting [183]. Using a pre-trained CNN on a natural image or varied medical image modalities, and then, fine-tuning on the medical images can be a possible solution to this problem [184].

Norman et al. [185] used the 2D U-Net proposed by Ronneberger et al. [186] to segment various sub-compartments of the knee, including articular cartilage and meniscus. The authors reported 86.7% mean validation (of 37 subjects) DSC on OAI dataset. The datasets applied for training and validation were divided into two sets: patients with OA (i.e., Kellgren-Lawrence (KL) [187] score > 1) and patients whose condition was longitudinally stable (i.e., KL score = $[0 - 1]$). The 2D U-Net has been designed to perform pixel-wise classification of high-resolution images. Liu et al. [188] applied 2D SegNet [189] for bone and cartilage segmentation on SKI10 dataset, and further compared the results with U-Net, which demonstrated that SegNet is more capable of segmenting musculoskeletal images in terms of accuracy and computational efficiency. After applying 3D simplex deformable modelling, the algorithm allows smooth deformation of bone and cartilage boundaries. Thus, the algorithm ascertains boundary smoothness and preserves the overall shape of knee sub-compartments. Their method was ranked second with 64.1 ± 9.5 total score in SKI10 contest.

Meanwhile, Zhou et al. [190], inspired by the work reported in [188], by combining the CNN model with conditional random field (CRF) with spatial proximity, as an additional post-processing step to finalise the labels. The authors reported more than 80% of DSC for all cartilages.

Table 10: Summary of DL-based methods. Acronyms are from left to right (in order of appearance). Method: semi-automatic (SA), fully automatic (FA). Dataset: number (#) of subjects (healthy asymptomatic (h) / patients having symptomatic knees (p)). Metrics: Dice similarity coefficient (DSC), specificity (SP), sensitivity (SN), volumetric overlap error (VOE), root-mean-square symmetric surface distance (RMSD). These metrics can be calculated on the knee compartments: medial tibial cartilage (cMT), patellar cartilage (cPT), total femoral cartilage (cF), lateral tibial cartilage (cLT), total tibial cartilage (cT), femur bone (bF), tibia bone (bT).

Method (SA/FA)	Network architecture	MR pulse sequence	Dataset # subjects (h/p)	Metrics
Triplanar-CNN [181] (FA)	three 2D-CNNs	Turbo 3D-T1	in-house train:25 (h,p) test:114 (h,p)	$DSC_{cMT} = 82.49\%$ $SN = 81.92\%$ $SP = 99.97\%$
pixel-wise classification on 2D sagittal plane [185] (FA)	2D U-Net	WE 3D-DESS	OAI (174) train:121 (h,p) validation:37 (h,p) test:16 (h,p)	$DSC = 86.7\%$
Slice-wise segmentation +3D Simplex deformable model [188] (FA)	2D SegNet	Many (T1, T2, etc.)	SKI10 train:60 (h,p) test:40 (h,p)	$VOE_{cF} = 28.4\%$ $VOE_{cT} = 33.1\%$ $RMSD_{bF} = 1.08$ mm $RMSD_{bT} = 1.09$ mm
SegNet+ CRF +3D Simplex deformable model [190] (FA)	2D SegNet	FS 3D-FSE	in-house 20p (leave-one-out)	$DSC_{cPT} = 80.7\%$ $DSC_{cT} = 80.1\%$ $DSC_{cF} = 80.6\%$
Combined SSMs and CNNs (2D U-Net + SSMs + 3D U-Net + SSMs) [191] (FA)	2D U-Net & 3D U-Net	Many (T1, T2, etc.)	SKI10 train:60 (h,p) test:40 (h,p)	$VOE_{cF} = 20.99\%$ $VOE_{cT} = 19.06\%$ $RMSD_{bF} = 0.74$ mm $RMSD_{bT} = 0.59$ mm

Continued...

Table 10 Continued...

Method (SA/FA)	Network architecture	MR pulse sequence	Dataset # subjects (h/p)	Metrics
		WE 3D-DESS	OAI-Imorphics (176) train:88 (h,p) test:88 (h,p)	$DSC_{cF} = 89.1\%$ $DSC_{cMT} = 85.8\%$ $DSC_{cLT} = 90\%$
		WE 3D-DESS	OAI-ZIB (507) train:253 (h,p) test:254 (h,p)	$DSC_{cF} = 89.9\%$ $DSC_{cT} = 85.6\%$

While DL-based approaches have been successful in segmenting medical images, they fail to discard outliers during segmentation. Besides, modelling the patient-specific shape variability of bone and cartilage in OA patients (with small and local shape variation in pathological data) is a challenging task. The segmentation model cannot clearly outline the areas of low contrast or imaging artefacts, which may result in inaccuracies during inference. Ambellan et al. [191] embedded SSMs adjustment into 2D and 3D CNNs, as a post-processing step, where SSMs correct the segmentation outcomes obtained after each CNN model to fill the holes and sub-holes in the segmentation mask from the previous step. The authors reported the best results of all published work on the validation data of SKI10 dataset, which recorded 20.99% and 19.06% VOE of cF and cT, respectively; outperforming the findings depicted in [171] (see Table 9). The SSMs were constructed from the bones on SKI10 to obtain bone segmentation for OAI dataset since OAI has no manual segmentation of bones. Overall, the combination of SSMs and CNNs achieved up to 88.3% of DSC on OAI validation set, including a 12-month follow-up dataset.

Ambellan et al. [191] combined 2D and 3D U-Nets, and made use of two different datasets of OAI images. They are referred to as OAI-Imorphics and OAI-ZIB, comprising 176 and 507 volumes. This method achieved a DSC value of 85.8% – 90% and 85.6% – 89.9% for each dataset respectively. Two-dimensional convolutional filters in 2D CNNs limits the spatial consistency in 3D knee MRIs. In order to increase the spatial consistency of segmentation outcomes, Ambellan et al. [191] added 8 adjacent slices of an individual slice to train the CNNs with 17 input channels.

Most of the DL methods applied for musculoskeletal structure segmentation have been based on 2D CNNs that employ 2D convolutions on sagittal orthogonal view in a slice-wise segmentation manner [185, 188, 190]. The main reason for this is the limited GPU memory, thus resulting in a limited spatial context within the 3D patch-based CNN approaches.

4. Discussion and concluding remarks

In this survey on knee articular cartilage segmentation methods in MRIs, we have discussed a classification of the state-of-the-art strategies with regard to the method applied, databases, and quantitative results. We have identified six main categories. The first category, conventional segmentation methods, includes region-growing, WST, and edge-based strategies. The second category comprises ACMs (which include B-spline and snakes). All of these techniques are performed interactively or semi-automatically and validated mostly on healthy subjects. However, In the next category, we have discussed SSMs that typically require a training dataset (i.e., shape model) to estimate the geometrical representation of the knee structure. Graph-based and atlas-based strategies are the next two categories and finally, the last category includes learning-based methods, which are subdivided into classical machine learning algorithms based on hand-crafted features, and emerging machine learning techniques referred to as DL models based on self-learning features.

As noticed from the summary tables, a comparison of the methods is not an easy task. Lack of standard databases and unified benchmarks are the main challenges. Moreover, it is not straightforward to compare the methods and evaluate based on their reported experimental results due to different testing datasets. These results thus need to be interpreted with caution, mainly because the accuracy of the segmentation method strongly depends on the dataset. To represent this issue, we have selected two publicly available datasets (SKI10 and OAI), with varying degree of KOA severity.

A large number of publications on knee joint segmentation methods have been used alone or in combination with other strategies. Hybrid methods have demonstrated good results [141, 155, 179, 171]. Thus, it is possible to combine learning-based methods with other methods to enhance the segmentation outcomes. Hierarchical learning-based scheme combined with geometric graph-based method allows segmentation of bone and cartilage simultaneously [155]. Given the fact that multiple atlas-based methods offer spatial prior of the anatomical structures, multiple atlas [157] or a combination of this method with any other method [179, 171] provides good results for the thin structure of cartilages.

This review has shown that learning-based methods dominate the field of knee cartilage segmentation. To the best of our knowledge, supervised learning-based techniques like k -NN [171], SVM [176], and AdaBoost [154, 155] are used for knee articular cartilage segmentation. A trend seems to exist on the use of DL strategies, either as an individual segmentation method [185] or combined with other approaches [190]. DL-based segmentation techniques can achieve acceptable overall performance, when compared to atlas-based [171] and model-based methods [140] since they are computationally costly. Therefore, researchers are recommended to conduct combined DL-based models and any other method that can attain better accuracy levels, when compared to those reported in existing studies. The combination of UNet and LOGISMOS has shown significant improvement for pancreas segmentation, in comparison to UNet and/or LOGISMOS on its own [192]. A similar strategy can be used for knee articular cartilage segmentation. Thus, it would be beneficial to adapt curvature and shape data into the DL-based model.

Many image analysis tools have been developed over the years to automate the knee joint segmentation. The Imorphics (based in Manchester, UK) has developed an image analysis tool based on 3D statistical shape models for fully-automated segmentation of knee bone and cartilage from MR images. Imorphics resulted in state of the art in terms of speed, precision and accuracy in automatic segmentation. Since 2007, LOGISMOS³ image segmentation framework is developed (at the Iowa Institute for Biomedical Imaging (IIBI)) as multiple objects and surfaces that can be applied on 2, 3, and 4D data; however, the framework still requires considerable manual correction. Another framework for the quantitative evaluation of cartilage biomarkers, the ArthroVision⁴, involves determining KOA progression and also provides the technology to analyse the morphological and structural changes in other tissues such as meniscus and subchondral bone. Regarding future work, development of a useful tool based on CNNs for assessing the morphological and structural changes in the musculoskeletal system can be an interesting research field for aiding the clinical application, particularly for longitudinal assessments. The design and development of 3D CNNs learning-based framework for the graph representation of the knee joints that can accommodate both edge and shape information for the graph can be served for future research.

Analysing the literature, we observe that issues of inter- and intra-radiologist disagreements should be weighed in during validation. Segmentation techniques have been mostly performed interactively in early work. Thus, the fundamental methods have been validated by measuring the reproducibility of ThC, VC, and tAB in paired datasets to assess the quality of interactive segmentation methods. Additionally, self-assessment is not a reliable validation method [41].

The development of DL-based algorithms offers better modelling of medical image data and segmentation of knee MRI. One major advantage of DL algorithms is that it learns the contextual features automatically without requiring any conventional high computational spatial structure modelling, such as atlas-based and model-based methods. In this paper, we provided an updated review with a focus on DL application in knee articular cartilage segmentation. Nevertheless, there is still a need for investigations to improve the present algorithms to deal with the challenges such as lack of thorough assessment for clinical practices and the intensity inhomogeneity.

References

- [1] M. Cross, E. Smith, D. Hoy, S. Nolte, I. Ackerman, M. Fransen, L. Bridgett, S. Williams, F. Guillemin, C. L. Hill, L. L. Laslett, G. Jones, F. Cicuttini, R. Osborne, T. Vos, R. Buchbinder, A. Woolf, L. March, The global burden of hip and knee osteoarthritis: estimates from the global burden of disease 2010 study, *Annals of the Rheumatic Diseases* 73 (7) (2014) 1323–1330.
- [2] E. R. Vina, C. K. Kwok, Epidemiology of osteoarthritis: literature update, *Current opinion in rheumatology* 30 (2) (2018) 160–167.
- [3] T. Neogi, The epidemiology and impact of pain in osteoarthritis, *Osteoarthritis and Cartilage* 21 (9) (2013) 1145 – 1153, pain in Osteoarthritis.

³<https://www.iibi.uiowa.edu/logismos>

⁴https://www.arthrolab.com/en/int_01_01.html

- [4] P. A. Dieppe, L. S. Lohmander, Pathogenesis and management of pain in osteoarthritis, *The Lancet* 365 (9463) (2005) 965 – 973.
- [5] F. Eckstein, F. Cicuttini, J.-P. Raynauld, J. Waterton, C. Peterfy, Magnetic resonance imaging (mri) of articular cartilage in knee osteoarthritis (oa): morphological assessment, *Osteoarthritis and Cartilage* 14 (2006) 46 – 75.
- [6] L. M. March, H. Bagga, Epidemiology of osteoarthritis in australia, *Medical Journal of Australia* 180 (5) (2004) S6–S10.
- [7] S. Kurtz, K. Ong, E. Lau, F. Mowat, M. Halpern, Projections of primary and revision hip and knee arthroplasty in the united states from 2005 to 2030, *JBJS* 89 (4) (2007) 780–785.
- [8] S. J. A., Y. Shaohua, Septic arthritis in emergency departments in the us: A national study of health care utilization and time trends, *Arthritis Care & Research* 70 (2) (2018) 320–326.
- [9] A. Berger, K. Bozic, B. Stacey, J. Edelsberg, A. Sadosky, G. Oster, Patterns of pharmacotherapy and health care utilization and costs prior to total hip or total knee replacement in patients with osteoarthritis, *Arthritis & Rheumatism* 63 (8) (2011) 2268–2275.
- [10] B. Sharif, J. A. Kopec, H. Wong, A. H. Anis, Distribution and drivers of average direct cost of osteoarthritis in canada from 2003 to 2010, *Arthritis care & research* 69 (2) (2017) 243–251.
- [11] F. Xie, B. Kovic, X. Jin, X. He, M. Wang, C. Silvestre, Economic and humanistic burden of osteoarthritis: a systematic review of large sample studies, *Pharmacoeconomics* 34 (11) (2016) 1087–1100.
- [12] H. J. Braun, G. E. Gold, Diagnosis of osteoarthritis: imaging, *Bone* 51 (2) (2012) 278–288.
- [13] N. Hafezi-Nejad, S. Demehri, A. Guermazi, J. A. Carrino, Osteoarthritis year in review 2017: updates on imaging advancements, *Osteoarthritis and Cartilage* 26 (3) (2018) 341–349.
- [14] A. Guermazi, F. Roemer, H. Genant, Role of imaging in osteoarthritis: diagnosis, prognosis, and follow-up, *Medicographia* 35 (2) (2013) 164–171.
- [15] X. Wang, D. Hunter, X. Jin, C. Ding, The importance of synovial inflammation in osteoarthritis: current evidence from imaging assessments and clinical trials, *Osteoarthritis and Cartilage* 26 (2) (2018) 165 – 174.
- [16] F. W. Roemer, F. Eckstein, D. Hayashi, A. Guermazi, The role of imaging in osteoarthritis, *Best Practice & Research Clinical Rheumatology* 28 (1) (2014) 31–60, osteoarthritis: Moving from Evidence to Practice.
- [17] A. J. R. Palmer, C. P. Brown, E. G. McNally, A. J. Price, I. Tracey, P. Jeppard, A. J. Carr, S. Glyn-Jones, Non-invasive imaging of cartilage in early osteoarthritis, *The Bone & Joint Journal* 95-B (6) (2013) 738–746.
- [18] F. W. Roemer, M. D. Crema, S. Trattnig, A. Guermazi, Advances in imaging of osteoarthritis and cartilage, *Radiology* 260 (2) (2011) 332–354.
- [19] Y. Wang, A. E. Wluka, G. Jones, C. Ding, F. M. Cicuttini, Use magnetic resonance imaging to assess articular cartilage, *Therapeutic Advances in Musculoskeletal Disease* 4 (2) (2012) 77–97.
- [20] D. T. Felson, M. C. Nevitt, M. Yang, M. Clancy, J. Niu, J. C. Torner, C. E. Lewis, P. Aliabadi, B. Sack, C. McCulloch, Y. Zhang, A new approach yields high rates of radiographic progression in knee osteoarthritis, *The Journal of Rheumatology* 35 (10) (2008) 2047–2054.
- [21] A. Guermazi, F. W. Roemer, D. Burstein, D. Hayashi, Why radiography should no longer be considered a surrogate outcome measure for longitudinal assessment of cartilage in knee osteoarthritis, *Arthritis Research & Therapy* 13 (6) (2011) 247.
- [22] M. D. Crema, F. W. Roemer, M. D. Marra, D. Burstein, G. E. Gold, F. Eckstein, T. Baum, T. J. Mosher, J. A. Carrino, A. Guermazi, Articular cartilage in the knee: Current mr imaging techniques and applications in clinical practice and research, *RadioGraphics* 31 (1) (2011) 37–61.
- [23] D. Kumar, A. Gandhamal, S. Talbar, A. F. M. Hani, Knee articular cartilage segmentation from mr images: A review, *ACM Comput. Surv.* 51 (5) (2018) 97:1–97:29.
- [24] S. Banerjee, R. Krug, J. Carballido-Gamio, D. A. Kelley, D. Xu, D. B. Vigneron, S. Majumdar, Rapid in vivo musculoskeletal mr with parallel imaging at 7t, *Magnetic Resonance in Medicine* 59 (3) (2008) 655–660.
- [25] H. Sittek, F. Eckstein, A. Gavazzeni, S. Milz, B. Kiefer, E. Schulte, M. Reiser, Assessment of normal patellar cartilage volume and thickness using mri: an analysis of currently available pulse sequences, *Skeletal Radiology* 25 (1) (1996) 55–62.
- [26] V. Juras, V. Mlynarik, P. Szomolanyi, L. Valkovič, S. Trattnig, Magnetic resonance imaging of the musculoskeletal system at 7t: Morphological imaging and beyond, *Top Magn Reson Imaging* 28 (3) (2019) 125–135.
- [27] J. Cheong, D. Suter, F. Cicuttini, Development of semi-automatic segmentation methods for measuring tibial cartilage volume, in: *Digital Image Computing: Techniques and Applications, 2005. DICTA'05. Proceedings 2005, IEEE, 2005*, pp. 45–45.
- [28] P. R. Kornaat, R. Y. Ceulemans, H. M. Kroon, N. Riyazi, M. Kloppenburg, W. O. Carter, T. G. Woodworth, J. L. Bloem, Mri assessment of knee osteoarthritis: Knee osteoarthritis scoring system (koss)—inter-observer and intra-observer reproducibility of a compartment-based scoring system, *Skeletal radiology* 34 (2) (2005) 95–102.
- [29] D. J. Hunter, G. H. Lo, D. Gale, A. J. Grainger, A. Guermazi, P. G. Conaghan, The reliability of a new scoring system for knee osteoarthritis mri and the validity of bone marrow lesion assessment: Bloks (boston–leeds osteoarthritis knee score), *Annals of the Rheumatic Diseases* 67 (2) (2008) 206–211.
- [30] D. J. Hunter, A. Guermazi, G. H. Lo, A. J. Grainger, P. G. Conaghan, R. M. Boudreau, F. W. Roemer, Evolution of semi-quantitative whole joint assessment of knee oa: Moaks (mri osteoarthritis knee score), *Osteoarthritis Cartilage* 19 (8) (2011) 990–1002.
- [31] C. Peterfy, A. Guermazi, S. Zaim, P. Tirman, Y. Miaux, D. White, M. Kothari, Y. Lu, K. Fye, S. Zhao, H. Genant, Whole-organ magnetic resonance imaging score (worms) of the knee in osteoarthritis, *Osteoarthritis and Cartilage* 12 (3) (2004) 177 – 190.
- [32] R. J. Buck, B. T. Wyman, M.-P. H. Le Graverand, W. Wirth, F. Eckstein, A. Investigators, An efficient subset of morphological measures for articular cartilage in the healthy and diseased human knee, *Magnetic resonance in medicine* 63 (3) (2010) 680–690.
- [33] C. Peterfy, G. Gold, F. Eckstein, F. Cicuttini, B. Dardzinski, R. Stevens, Mri protocols for whole-organ assessment of the knee in osteoarthritis, *Osteoarthritis and Cartilage* 14 (2006) 95–111.
- [34] H. Wang, M. F. Koff, H. G. Potter, R. F. Warren, S. A. Rodeo, S. A. Maher, An mri-compatible loading device to assess knee joint cartilage deformation: Effect of preloading and inter-test repeatability, *Journal of Biomechanics* 48 (12) (2015) 2934 – 2940.
- [35] A. Arovitola, L. Gallo, Knee bone segmentation from mri: A classification and literature review, *Biocybernetics and Biomedical Engineering* 36 (2) (2016) 437 – 449.
- [36] V. Pedoia, S. Majumdar, T. M. Link, Segmentation of joint and musculoskeletal tissue in the study of arthritis, *Magnetic Resonance Materials in Physics, Biology and Medicine* 29 (2) (2016) 207–221.

- [37] J. Kubicek, M. Penhaker, M. Augustynek, I. Bryjova, M. Cerny, Segmentation of knee cartilage: A comprehensive review, *Journal of Medical Imaging and Health Informatics* 8 (3) (2018) 401–418.
- [38] B. Zhang, Y. Zhang, H.-D. Cheng, M. Xian, S. Gai, O. Cheng, K. Huang, Computer-aided knee joint magnetic resonance image segmentation—a survey, *arXiv preprint arXiv:1802.04894*.
- [39] Y. LeCun, Y. Bengio, G. Hinton, Deep learning, *nature* 521 (7553) (2015) 436.
- [40] F. Movahedi, J. L. Coyle, E. Sejdić, Deep belief networks for electroencephalography: A review of recent contributions and future outlooks, *IEEE Journal of Biomedical and Health Informatics* 22 (3) (2018) 642–652.
- [41] K. D. Toennies, *Guide to Medical Image Analysis: Methods and Algorithms*, Springer London, London, 2017.
- [42] C. Peterfy, C. Van Dijke, D. Janzen, C. Glüer, R. Namba, S. Majumdar, P. Lang, H. Genant, Quantification of articular cartilage in the knee with pulsed saturation transfer subtraction and fat-suppressed mr imaging: optimization and validation, *Radiology* 192 (2) (1994) 485–491.
- [43] A. A. Kshirsagar, P. J. Watson, J. A. Tyler, L. D. Hall, Measurement of localized cartilage volume and thickness of human knee joints by computer analysis of three-dimensional magnetic resonance images, *Investigative radiology* 33 (5) (1998) 289–299.
- [44] S. Ghosh, D. Newitt, S. Majumdar, Watershed segmentation of high resolution articular cartilage image, *International Society for Magnetic Resonance in Medicine*, Philadelphia.
- [45] T. Stammberger, F. Eckstein, M. Michaelis, K.-H. Englmeier, M. Reiser, Interobserver reproducibility of quantitative cartilage measurements: comparison of b-spline snakes and manual segmentation, *Magnetic Resonance Imaging* 17 (7) (1999) 1033 – 1042.
- [46] S. Solloway, C. J. Taylor, C. E. Hutchinson, J. C. Waterton, Quantification of articular cartilage from mr images using active shape models, in: *European Conference on Computer Vision*, Springer, 1996, pp. 400–411.
- [47] D. L. Pham, C. Xu, J. L. Prince, Current methods in medical image segmentation, *Annual Review of Biomedical Engineering* 2 (1) (2000) 315–337.
- [48] H. Shim, S. Lee, B. Kim, C. Tao, S. Chang, I. D. Yun, S. U. Lee, K. Kwok, K. Bae, 3-d segmentation of articular cartilages by graph cuts using knee mr images from osteoarthritis initiative, in: *Medical Imaging 2008: Image Processing*, Vol. 6914, International Society for Optics and Photonics, 2008, p. 691448.
- [49] J. G. Tamez-Peña, M. Barbu-McInnis, S. Totterman, Knee cartilage extraction and bone-cartilage interface analysis from 3d mri data sets, in: *Medical Imaging 2004: Image Processing*, Vol. 5370, International Society for Optics and Photonics, 2004, pp. 1774–1785.
- [50] J. Folkesson, E. Dam, O. F. Olsen, P. Pettersen, C. Christiansen, Automatic segmentation of the articular cartilage in knee mri using a hierarchical multi-class classification scheme, in: J. S. Duncan, G. Gerig (Eds.), *Medical Image Computing and Computer-Assisted Intervention – MICCAI 2005*, Springer Berlin Heidelberg, Berlin, Heidelberg, 2005, pp. 327–334.
- [51] T. Heimann, B. J. Morrison, M. A. Styner, M. Niethammer, S. Warfield, Segmentation of knee images: A grand challenge, in: *Proc. MICCAI Workshop on Medical Image Analysis for the Clinic*, 2010, pp. 207–214.
- [52] L. R. Dice, Measures of the amount of ecologic association between species, *Ecology* 26 (3) (1945) 297–302.
- [53] G. Vincent, C. Wolstenholme, I. Scott, M. Bowes, Fully automatic segmentation of the knee joint using active appearance models, *Medical Image Analysis for the Clinic: A Grand Challenge 1* (2010) 224.
- [54] Z. Ma, J. M. R. Tavares, R. N. Jorge, T. Mascarenhas, A review of algorithms for medical image segmentation and their applications to the female pelvic cavity, *Computer Methods in Biomechanics and Biomedical Engineering* 13 (2) (2010) 235–246.
- [55] C. Solomon, T. Breckon, *Fundamentals of Digital Image Processing: A practical approach with examples in Matlab*, John Wiley & Sons, 2011.
- [56] S. W. Zucker, Region growing: Childhood and adolescence, *Comput. Graph. Image Process.* 5 (1976) 382–399.
- [57] R. Adams, L. Bischof, Seeded region growing, *IEEE Transactions on Pattern Analysis and Machine Intelligence* 16 (6) (1994) 641–647.
- [58] K. W. Marshall, D. J. Mikulis, B. M. Guthrie, Quantitation of articular cartilage using magnetic resonance imaging and three-dimensional reconstruction, *Journal of Orthopaedic Research* 13 (6) (1995) 814–823.
- [59] F. Eckstein, A. Gavazzini, H. Sittek, M. Haubner, A. Lösch, S. Milz, K.-H. Englmeier, E. Schulte, R. Putz, M. Reiser, Determination of knee joint cartilage thickness using three-dimensional magnetic resonance chondro-crassometry (3d mr-ccm), *Magnetic Resonance in Medicine* 36 (2) (1996) 256–265.
- [60] M. Haubner, F. Eckstein, M. Schnier, A. Lösch, H. Sittek, C. Becker, H. Kolem, M. Reiser, K.-H. Englmeier, A non-invasive technique for 3-dimensional assessment of articular cartilage thickness based on mri part 2: Validation using ct arthrography, *Magnetic Resonance Imaging* 15 (7) (1997) 805 – 813.
- [61] A. Lösch, F. Eckstein, M. Haubner, K.-H. Englmeier, A non-invasive technique for 3-dimensional assessment of articular cartilage thickness based on mri part 1: Development of a computational method, *Magnetic Resonance Imaging* 15 (7) (1997) 795 – 804.
- [62] M. Tieschky, S. Faber, M. Haubner, H. Kolem, E. Schulte, K.-H. Englmeier, M. Reiser, F. Eckstein, Repeatability of patellar cartilage thickness patterns in the living, using a fat-suppressed magnetic resonance imaging sequence with short acquisition time and three-dimensional data processing, *Journal of orthopaedic research* 15 (6) (1997) 808–813.
- [63] F. Eckstein, M. Schnier, M. Haubner, J. Priebsch, C. Glaser, K.-H. Englmeier, M. Reiser, Accuracy of cartilage volume and thickness measurements with magnetic resonance imaging., *Clinical orthopaedics and related research* 198 (352) (1998) 137–148.
- [64] F. Eckstein, J. Westhoff, H. Sittek, K. Maag, M. Haubner, S. Faber, K. Englmeier, M. Reiser, In vivo reproducibility of three-dimensional cartilage volume and thickness measurements with mr imaging., *AJR. American journal of roentgenology* 170 (3) (1998) 593–597.
- [65] T. Stammberger, F. Eckstein, K.-H. Englmeier, M. Reiser, Determination of 3d cartilage thickness data from mr imaging: computational method and reproducibility in the living, *Magnetic resonance in medicine* 41 (3) (1999) 529–536.
- [66] S. K. Pakin, J. G. Tamez-Pena, S. Totterman, K. J. Parker, Segmentation, surface extraction, and thickness computation of articular cartilage, in: *Medical Imaging 2002: Image Processing*, Vol. 4684, International Society for Optics and Photonics, 2002, pp. 155–167.
- [67] J. G. Tamez-Peña, S. Totterman, K. J. Parker, Unsupervised statistical segmentation of multispectral volumetric mri images, in: *Medical Imaging 1999: Image Processing*, Vol. 3661, International Society for Optics and Photonics, 1999, pp. 300–312.
- [68] J.-M. Morel, S. Solimini, Variational methods in image segmentation, volume 14 of *progress in nonlinear differential equations and their applications*, Birkhauser Boston.
- [69] V. Grau, A. U. J. Mewes, M. Alcaniz, R. Kikinis, S. K. Warfield, Improved watershed transform for medical image segmentation using prior

- information, *IEEE Transactions on Medical Imaging* 23 (4) (2004) 447–458.
- [70] Y.-C. Lin, Y.-P. Tsai, Y.-P. Hung, Z.-C. Shih, Comparison between immersion-based and toboggan-based watershed image segmentation, *IEEE Transactions on Image Processing* 15 (3) (2006) 632–640.
- [71] P. Soille, L. Vincent, Watersheds in digital spaces: An efficient algorithm based on immersion simulations, *IEEE Transactions on Pattern Analysis & Machine Intelligence* 13 (1991) 583–598.
- [72] S. Ghosh, O. Beuf, M. Ries, N. E. Lane, L. S. Steinbach, T. M. Link, S. Majumdar, Watershed segmentation of high resolution magnetic resonance images of articular cartilage of the knee, in: *Proceedings of the 22nd Annual International Conference of the IEEE Engineering in Medicine and Biology Society (Cat. No.00CH37143)*, Vol. 4, 2000, pp. 3174–3176.
- [73] S. Ghosh, M. Ries, N. Lane, C. Ghajar, S. Majumdar, Segmentation of high resolution articular cartilage mr images, *Trans Orthoped Res Soc (ORS)* 246.
- [74] J. Besag, On the statistical analysis of dirty pictures, *Journal of the Royal Statistical Society. Series B (Methodological)* 48 (3) (1986) 259–302.
- [75] E. B. Dam, J. Folkesson, P. C. Pettersen, C. Christiansen, Semi-automatic knee cartilage segmentation, in: *Medical Imaging 2006: Image Processing*, Vol. 6144, International Society for Optics and Photonics, 2006, pp. 614441–614449.
- [76] J. Canny, A computational approach to edge detection, *IEEE Transactions on Pattern Analysis and Machine Intelligence PAMI-8* (6) (1986) 679–698.
- [77] M. S. M. Swamy, M. S. Holi, Segmentation, visualization and quantification of knee joint articular cartilage using mr images, in: P. P. Swamy, D. S. Guru (Eds.), *Multimedia Processing, Communication and Computing Applications*, Springer India, New Delhi, 2013, pp. 321–332.
- [78] M. S. Mallikarjunaswamy, M. S. Holi, R. Raman, Quantification and 3d visualization of articular cartilage of knee joint using image processing techniques, in: L. C. Jain, H. S. Behera, J. K. Mandal, D. P. Mohapatra (Eds.), *Computational Intelligence in Data Mining - Volume 2*, Springer India, New Delhi, 2015, pp. 417–425.
- [79] M. S. M. Swamy, M. S. Holi, Knee joint cartilage visualization and quantification in normal and osteoarthritis, in: *2010 International Conference on Systems in Medicine and Biology*, 2010, pp. 138–142.
- [80] S. Kubakaddi, K. Ravikumar, H. DG, Measurement of cartilage thickness for early detection of knee osteoarthritis (koa), in: *2013 IEEE Point-of-Care Healthcare Technologies (PHT)*, 2013, pp. 208–211.
- [81] J. Carballido-Gamio, J. S. Bauer, K.-Y. Lee, S. Krause, S. Majumdar, Combined image processing techniques for characterization of mri cartilage of the knee, in: *2005 IEEE Engineering in Medicine and Biology 27th Annual Conference*, 2005, pp. 3043–3046.
- [82] S. A. A. Shah, K. M. Yahya, G. Mubashar, A. Bais, Quantification and visualization of mri cartilage of the knee: A simplified approach, in: *2010 6th International Conference on Emerging Technologies (ICET)*, 2010, pp. 175–180.
- [83] P. M. M. Cashman, R. I. Kitney, M. A. Gariba, M. E. Carter, Automated techniques for visualization and mapping of articular cartilage in mr images of the osteoarthritic knee: a base technique for the assessment of microdamage and submicro damage, *IEEE Transactions on NanoBioscience* 99 (1) (2002) 42–51.
- [84] C. . Poh, R. I. Kitney, Viewing interfaces for segmentation and measurement results, in: *2005 IEEE Engineering in Medicine and Biology 27th Annual Conference*, 2005, pp. 5132–5135.
- [85] M. M. Swamy, M. S. Holi, Knee joint articular cartilage segmentation using radial search method, visualization and quantification, *International Journal of Biometrics and Bioinformatics (IJBB)* 7 (1) (2013) 1.
- [86] S. Akhtar, C. Poh, R. Kitney, An mri derived articular cartilage visualization framework, *Osteoarthritis and Cartilage* 15 (9) (2007) 1070 – 1085.
- [87] K. Chang, L. Chen, C. Wu, S. Chen, Articular cartilage segmentation based on radial transformation, in: *Hybrid Intelligent Systems, International Conference on (HIS)*, Vol. 01, 2009, pp. 239–242.
- [88] M. K. Liukkonen, M. E. Mononen, P. Tanska, S. Saarakkala, M. T. Nieminen, R. K. Korhonen, Application of a semi-automatic cartilage segmentation method for biomechanical modeling of the knee joint, *Computer Methods in Biomechanics and Biomedical Engineering* 20 (13) (2017) 1453–1463.
- [89] P. Dodin, J. Martel-Pelletier, J.-P. Pelletier, F. Abram, A fully automated human knee 3d mri bone segmentation using the ray casting technique, *Medical & Biological Engineering & Computing* 49 (12) (2011) 1413–1424.
- [90] J. Kubicek, M. Penhaker, I. Bryjova, M. Kodaj, Articular cartilage defect detection based on image segmentation with colour mapping, in: D. Hwang, J. J. Jung, N.-T. Nguyen (Eds.), *Computational Collective Intelligence. Technologies and Applications*, Springer International Publishing, Cham, 2014, pp. 214–222.
- [91] J. Kubicek, M. Augustynek, M. Penhaker, I. Bryjova, L. Peter, Multiregional fuzzy thresholding segmentation completed by spatial median aggregation: Modeling and segmentation of early pathological findings of articular cartilage, in: H. Eskola, O. Väisänen, J. Viik, J. Hyttinen (Eds.), *EMBEC & NBC 2017*, Springer Singapore, Singapore, 2018, pp. 876–879.
- [92] N. Otsu, A. Threshold, Selection method from gray-level histograms, *IEEE Trans, SMC9*, 1989 (1) 62–66.
- [93] S. Aja-Fernández, A. H. Curiale, G. Vegas-Sánchez-Ferrero, A local fuzzy thresholding methodology for multiregion image segmentation, *Knowledge-Based Systems* 83 (2015) 1 – 12.
- [94] J. C. Bezdek, R. Ehrlich, W. Full, Fcm: The fuzzy c-means clustering algorithm, *Computers & Geosciences* 10 (2) (1984) 191 – 203.
- [95] T. McInerney, D. Terzopoulos, Deformable models in medical image analysis, in: *Proceedings of the Workshop on Mathematical Methods in Biomedical Image Analysis*, 1996, pp. 171–180.
- [96] Y. Sun, E. C. Teo, Q. H. Zhang, Discussions of knee joint segmentation, in: *2006 International Conference on Biomedical and Pharmaceutical Engineering*, 2006, p. 2006.
- [97] Y. Chi, P. Cashman, R. Kitney, Automatic segmentation of cartilage in mr images using cdcg: Chessboard directional compensated gvf snakes, in: *International Conference on Medical Information Visualisation - BioMedical Visualisation (MedVis'06)*, 2006, pp. 45–50.
- [98] Y. Chi, R. I. Kitney, P. Cashman, Automatic cartilage detection in mr image sets using cdsg snake, in: R. Magjarevic, J. H. Nagel (Eds.), *World Congress on Medical Physics and Biomedical Engineering 2006*, Springer Berlin Heidelberg, Berlin, Heidelberg, 2007, pp. 2398–2402.

- [99] M. Kass, A. Witkin, D. Terzopoulos, Snakes: Active contour models, *International Journal of Computer Vision* 1 (4) (1988) 321–331.
- [100] P. Kornaat, S. Reeder, S. Koo, J. Brittain, H. Yu, T. Andriacchi, G. Gold, Mr imaging of articular cartilage at 1.5t and 3.0t: Comparison of spgr and ssfp sequences, *Osteoarthritis and Cartilage* 13 (4) (2005) 338 – 344.
- [101] J. Carballido-Gamio, J. S. Bauer, R. Stahl, K.-Y. Lee, S. Krause, T. M. Link, S. Majumdar, Inter-subject comparison of mri knee cartilage thickness, *Medical Image Analysis* 12 (2) (2008) 120 – 135.
- [102] E. Ozhinksy, S. Majumdar, 3d visualization of cartilage thickness in knee joint using bezier spline segmentation, in: *Eleventh Annual Scientific Meeting of the International Society for Magnetic Resonance in Medicine (ISMRM)*, 2003, pp. 10–16.
- [103] J. Carballido-Gamio, G. B. Joseph, J. A. Lynch, T. M. Link, S. Majumdar, Longitudinal analysis of mri t2 knee cartilage laminar organization in a subset of patients from the osteoarthritis initiative: A texture approach, *Magnetic Resonance in Medicine* 65 (4) (2011) 1184–1194.
- [104] J. C. Russ, *The image processing handbook*, CRC press, 2016.
- [105] Z. A. Cohen, D. M. McCarthy, S. D. Kwak, P. Legrand, F. Fogarasi, E. J. Ciaccio, G. A. Ateshian, Knee cartilage topography, thickness, and contact areas from mri: in-vitro calibration and in-vivo measurements, *Osteoarthritis and cartilage* 7 (1) (1999) 95–109.
- [106] J. A. Lynch, S. Zaim, J. Zhao, A. Stork, C. G. Peterfy, H. K. Genant, Cartilage segmentation of 3d mri scans of the osteoarthritic knee combining user knowledge and active contours, in: *Medical Imaging 2000, International Society for Optics and Photonics*, 2000, pp. 925–935.
- [107] J. A. Lynch, S. Zaim, J. Zhao, C. G. Peterfy, H. K. Genant, Automating measurement of subtle changes in articular cartilage from mri of the knee by combining 3d image registration and segmentation, in: *Medical Imaging 2001: Image Processing*, Vol. 4322, International Society for Optics and Photonics, 2001, pp. 431–440.
- [108] M. Fornefett, K. Rohr, H. Stiehl, Radial basis functions with compact support for elastic registration of medical images, *Image and Vision Computing* 19 (1) (2001) 87 – 96.
- [109] P. J. Besl, N. D. McKay, Method for registration of 3-d shapes, in: *Sensor Fusion IV: Control Paradigms and Data Structures*, Vol. 1611, International Society for Optics and Photonics, 1992, pp. 586–607.
- [110] C. Kauffmann, P. Gravel, B. Godbout, A. Gravel, G. Beaudoin, J. . Raynauld, J. Martel-Pelletier, J. . Pelletier, J. A. de Guise, Computer-aided method for quantification of cartilage thickness and volume changes using mri: validation study using a synthetic model, *IEEE Transactions on Biomedical Engineering* 50 (8) (2003) 978–988.
- [111] J.-P. Raynauld, C. Kauffmann, G. Beaudoin, M.-J. Berthiaume, J. A. de Guise, D. Bloch, F. Camacho, B. Godbout, R. Altman, M. Hochberg, et al., Reliability of a quantification imaging system using magnetic resonance images to measure cartilage thickness and volume in human normal and osteoarthritic knees, *Osteoarthritis and cartilage* 11 (5) (2003) 351–360.
- [112] J. Duryea, G. Neumann, M. Brem, W. Koh, F. Noorbakhsh, R. Jackson, J. Yu, C. Eaton, P. Lang, Novel fast semi-automated software to segment cartilage for knee mr acquisitions, *Osteoarthritis and Cartilage* 15 (5) (2007) 487 – 492.
- [113] M. H. Brem, J. Pauser, H. Yoshioka, A. Brenning, J. Stratmann, F. F. Hennig, R. Kikinis, J. Duryea, C. S. Winalski, P. Lang, Longitudinal in vivo reproducibility of cartilage volume and surface in osteoarthritis of the knee, *Skeletal Radiology* 36 (4) (2007) 315–320.
- [114] M. H. Brem, P. K. Lang, G. Neumann, P. M. Schlechtweg, E. Schneider, R. Jackson, J. Yu, C. B. Eaton, F. F. Hennig, H. Yoshioka, G. Pappas, J. Duryea, Magnetic resonance image segmentation using semi-automated software for quantification of knee articular cartilage—initial evaluation of a technique for paired scans, *Skeletal Radiology* 38 (5) (2009) 505–511.
- [115] J. Tang, S. Millington, S. T. Acton, J. Crandall, S. Hurwitz, Surface extraction and thickness measurement of the articular cartilage from mr images using directional gradient vector flow snakes, *IEEE Transactions on Biomedical Engineering* 53 (5) (2006) 896–907.
- [116] T. Iranpour-Boroujeni, A. Watanabe, R. Bashtar, H. Yoshioka, J. Duryea, Quantification of cartilage loss in local regions of knee joints using semi-automated segmentation software: analysis of longitudinal data from the osteoarthritis initiative (oai), *Osteoarthritis and Cartilage* 19 (3) (2011) 309 – 314.
- [117] C. Xu, J. L. Prince, Snakes, shapes, and gradient vector flow, *IEEE Transactions on Image Processing* 7 (3) (1998) 359–369.
- [118] T. Heimann, H.-P. Meinzer, Statistical shape models for 3d medical image segmentation: A review, *Medical Image Analysis* 13 (4) (2009) 543 – 563.
- [119] T. Cootes, E. Baldock, J. Graham, An introduction to active shape models, *Image processing and analysis* (2000) 223–248.
- [120] T. F. Cootes, C. J. Taylor, Active shape models — ‘smart snakes’, in: D. Hogg, R. Boyle (Eds.), *BMVC92*, Springer London, London, 1992, pp. 266–275.
- [121] T. F. Cootes, C. J. Taylor, Constrained active appearance models, in: *Proceedings Eighth IEEE International Conference on Computer Vision. ICCV 2001*, Vol. 1, 2001, pp. 748–754 vol.1.
- [122] G. Chintalapani, L. M. Ellingsen, O. Sadovsky, J. L. Prince, R. H. Taylor, Statistical atlases of bone anatomy: construction, iterative improvement and validation, in: *International Conference on Medical Image Computing and Computer-Assisted Intervention*, Springer, 2007, pp. 499–506.
- [123] W. E. Lorensen, H. E. Cline, Marching cubes: A high resolution 3d surface construction algorithm, *SIGGRAPH Comput. Graph.* 21 (4) (1987) 163–169.
- [124] C. Goodall, Procrustes methods in the statistical analysis of shape, *Journal of the Royal Statistical Society. Series B (Methodological)* 53 (2) (1991) 285–339.
- [125] I. Jolliffe, Principal component analysis, in: *International encyclopedia of statistical science*, Springer Berlin Heidelberg, 2011, pp. 1094–1096.
- [126] J. Fripp, P. Bourgeat, A. J. Mewes, S. K. Warfield, S. Crozier, S. Ourselin, 3d statistical shape models to embed spatial relationship information, in: *International Workshop on Computer Vision for Biomedical Image Applications*, Springer, 2005, pp. 51–60.
- [127] T. F. Cootes, C. J. Taylor, Using grey-level models to improve active shape model search, in: *Proceedings of 12th International Conference on Pattern Recognition*, Vol. 1, 1994, pp. 63–67 vol.1.
- [128] S. Solloway, C. E. Hutchinson, J. C. Waterton, C. J. Taylor, The use of active shape models for making thickness measurements of articular cartilage from mr images, *Magnetic Resonance in Medicine* 37 (6) (1997) 943–952.
- [129] G. González, B. Escalante-Ramírez, Knee cartilage segmentation using active shape models and local binary patterns, in: *Optics, Photonics, and Digital Technologies for Multimedia Applications III*, Vol. 9138, International Society for Optics and Photonics, 2014, p. 91380K.

- [130] G. González, B. Escalante-Ramírez, Knee cartilage segmentation using active shape models and contrast enhancement from magnetic resonance images, in: IX International Seminar on Medical Information Processing and Analysis, Vol. 8922, International Society for Optics and Photonics, 2013, p. 892213.
- [131] J. Fripp, S. Crozier, S. Warfield, S. Ourselin, Automatic initialization of 3d deformable models for cartilage segmentation, in: Digital Image Computing: Techniques and Applications (DICTA'05), 2005, pp. 74–74.
- [132] T. Möller, B. Trumbore, Fast, minimum storage ray/triangle intersection, in: ACM SIGGRAPH 2005 Courses, SIGGRAPH '05, ACM, New York, NY, USA, 2005, p. 7.
- [133] J. Fripp, S. Crozier, S. K. Warfield, S. Ourselin, Automatic segmentation of the bone and extraction of the bone–cartilage interface from magnetic resonance images of the knee, *Physics in Medicine & Biology* 52 (6) (2007) 1617.
- [134] J. Fripp, S. Crozier, S. K. Warfield, S. Ourselin, Automatic segmentation of articular cartilage in magnetic resonance images of the knee, in: N. Ayache, S. Ourselin, A. Maeder (Eds.), *Medical Image Computing and Computer-Assisted Intervention – MICCAI 2007*, Springer Berlin Heidelberg, Berlin, Heidelberg, 2007, pp. 186–194.
- [135] S. Ourselin, A. Roche, G. Subsol, X. Pennec, N. Ayache, Reconstructing a 3d structure from serial histological sections, *Image and Vision Computing* 19 (1) (2001) 25 – 31.
- [136] H. Seim, D. Kainmueller, H. Lamecker, M. Bindernagel, J. Malinowski, S. Zachow, Model-based auto-segmentation of knee bones and cartilage in mri data, *Medical Image Analysis for the Clinic: A Grand Challenge* (2010) 215–223.
- [137] J. A. Nelder, R. Mead, A simplex method for function minimization, *The Computer Journal* 7 (4) (1965) 308–313.
- [138] R. H. Davies, C. J. Twining, T. F. Cootes, J. C. Waterton, C. J. Taylor, 3d statistical shape models using direct optimisation of description length, in: A. Heyden, G. Sparr, M. Nielsen, P. Johansen (Eds.), *Computer Vision — ECCV 2002*, Springer Berlin Heidelberg, Berlin, Heidelberg, 2002, pp. 3–20.
- [139] T. G. Williams, A. Holmes, J. C. Waterton, R. A. Maciewicz, A. F. Nash, C. J. Taylor, Regional quantitative analysis of knee cartilage in a population study using mri and model based correspondences., in: *ISBI, 2006*, pp. 311–314.
- [140] T. G. Williams, A. P. Holmes, J. C. Waterton, R. A. Maciewicz, C. E. Hutchinson, R. J. Moots, A. F. P. Nash, C. J. Taylor, Anatomically corresponded regional analysis of cartilage in asymptomatic and osteoarthritic knees by statistical shape modelling of the bone, *IEEE Transactions on Medical Imaging* 29 (8) (2010) 1541–1559.
- [141] J. Fripp, S. Crozier, S. K. Warfield, S. Ourselin, Automatic segmentation and quantitative analysis of the articular cartilages from magnetic resonance images of the knee, *IEEE transactions on medical imaging* 29 (1) (2010) 55–64.
- [142] Y. Y. Boykov, M. Jolly, Interactive graph cuts for optimal boundary segmentation of objects in n-d images, in: *Proceedings Eighth IEEE International Conference on Computer Vision, ICCV 2001, Vol. 1, 2001*, pp. 105–112 vol.1.
- [143] S. C. K. V. K. Govindan, A review on graph based segmentation, *International Journal of Image, Graphics and Signal Processing* 4 (5) (2012) 1–13, copyright - Copyright Modern Education and Computer Science Press Jun 2012; Last updated - 2014-11-30.
- [144] B. Peng, L. Zhang, D. Zhang, A survey of graph theoretical approaches to image segmentation, *Pattern Recognition* 46 (3) (2013) 1020 – 1038.
- [145] Z. Wu, R. Leahy, Tissue classification in mr images using hierarchical segmentation, in: *1990 IEEE Nuclear Science Symposium Conference Record, 1990*, pp. 1410–1414.
- [146] Y. Boykov, G. Funka-Lea, Graph cuts and efficient n-d image segmentation, *International Journal of Computer Vision* 70 (2) (2006) 109–131.
- [147] K. Bae, H. Shim, C. Tao, S. Chang, J. Wang, R. Boudreau, C. Kwok, Intra- and inter-observer reproducibility of volume measurement of knee cartilage segmented from the oai mr image set using a novel semi-automated segmentation method, *Osteoarthritis and Cartilage* 17 (12) (2009) 1589 – 1597.
- [148] H. Shim, S. Chang, C. Tao, J.-H. Wang, C. K. Kwok, K. T. Bae, Knee cartilage: Efficient and reproducible segmentation on high-spatial-resolution mr images with the semiautomated graph-cut algorithm method, *Radiology* 251 (2) (2009) 548–556.
- [149] S. Lee, H. Shim, S. H. Park, I. D. Yun, S. U. Lee, 3-d segmentation of knee bones on mr images by constrained branch-and-mincut, Program Committee • John Ashburner (University College London) • Sylvain Bouix (Harvard Medical School) • Tim Cootes (University of Manchester) (2009) 197.
- [150] S. Lee, H. Shim, S. H. Park, I. D. Yun, S. U. Lee, Learning local shape and appearance for segmentation of knee cartilage in 3d mri, in: *Proceedings of the 4th Medical Image Analysis for the Clinic—A Grand Challenge workshop (MICCAI 2010), 2010*, pp. 1710 – 1720.
- [151] S. Lee, S. H. Park, H. Shim, I. D. Yun, S. U. Lee, Optimization of local shape and appearance probabilities for segmentation of knee cartilage in 3-d mr images, *Computer Vision and Image Understanding* 115 (12) (2011) 1710 – 1720, special issue on Optimization for Vision, Graphics and Medical Imaging: Theory and Applications.
- [152] V. Lempitsky, A. Blake, C. Rother, Image segmentation by branch-and-mincut, in: D. Forsyth, P. Torr, A. Zisserman (Eds.), *Computer Vision – ECCV 2008*, Springer Berlin Heidelberg, Berlin, Heidelberg, 2008, pp. 15–29.
- [153] Y. Yin, X. Zhang, R. Williams, X. Wu, D. D. Anderson, M. Sonka, Logismos—layered optimal graph image segmentation of multiple objects and surfaces: Cartilage segmentation in the knee joint, *IEEE Transactions on Medical Imaging* 29 (12) (2010) 2023–2037.
- [154] S. Kashyap, I. Oguz, H. Zhang, M. Sonka, Automated segmentation of knee mri using hierarchical classifiers and just enough interaction based learning: Data from osteoarthritis initiative, in: S. Ourselin, L. Joskowicz, M. R. Sabuncu, G. Unal, W. Wells (Eds.), *Medical Image Computing and Computer-Assisted Intervention – MICCAI 2016*, Springer International Publishing, Cham, 2016, pp. 344–351.
- [155] S. Kashyap, H. Zhang, K. Rao, M. Sonka, Learning-based cost functions for 3-d and 4-d multi-surface multi-object segmentation of knee mri: Data from the osteoarthritis initiative, *IEEE Transactions on Medical Imaging* 37 (5) (2018) 1103–1113.
- [156] T. Rohlfing, R. Brandt, R. Menzel, D. B. Russakoff, C. R. Maurer, Quo vadis, atlas-based segmentation?, in: *Handbook of biomedical image analysis*, Springer, 2005, pp. 435–486.
- [157] L. Shan, C. Zach, C. Charles, M. Niethammer, Automatic atlas-based three-label cartilage segmentation from mr knee images, *Medical Image Analysis* 18 (7) (2014) 1233 – 1246.
- [158] J. G. Tamez-Peña, J. Farber, P. C. González, E. Schreyer, E. Schneider, S. Totterman, Unsupervised segmentation and quantification of anatomical knee features: Data from the osteoarthritis initiative, *IEEE Transactions on Biomedical Engineering* 59 (4) (2012) 1177–1186.
- [159] L. Shan, C. Zach, M. Styner, C. Charles, M. Niethammer, Automatic bone segmentation and alignment from mr knee images, in: *Medical*

- Imaging 2010: Image Processing, Vol. 7623, International Society for Optics and Photonics, 2010, p. 76231K.
- [160] L. Shan, C. Zach, M. Niethammer, Automatic three-label bone segmentation from knee mr images, in: 2010 IEEE International Symposium on Biomedical Imaging: From Nano to Macro, 2010, pp. 1325–1328.
- [161] L. Shan, M. Niethammer, Automatic atlas-based cartilage segmentation from knee mr images, in: Proc. MICCAI Workshop on Medical Image Analysis for the Clinic, 2011, pp. 241–246.
- [162] J.-G. Lee, S. Gumus, C. H. Moon, C. K. Kwok, K. T. Bae, Fully automated segmentation of cartilage from the mr images of knee using a multi-atlas and local structural analysis method, *Medical Physics* 41 (9) (2014) 092303.
- [163] J.-G. Lee, S. Gumus, K. Kwok, K. Bae, Fully-automated cartilage segmentation from magnetic resonance images of the knee using atlas and graph-cut algorithms, *Osteoarthritis and Cartilage* 21 (2013) S238–S239.
- [164] G. Litjens, T. Kooi, B. E. Bejnordi, A. A. A. Setio, F. Ciompi, M. Ghafoorian, J. A. van der Laak, B. van Ginneken, C. I. Sánchez, A survey on deep learning in medical image analysis, *Medical Image Analysis* 42 (2017) 60–88.
- [165] Y. LeCun, B. Boser, J. S. Denker, D. Henderson, R. E. Howard, W. Hubbard, L. D. Jackel, Backpropagation applied to handwritten zip code recognition, *Neural computation* 1 (4) (1989) 541–551.
- [166] O. Russakovsky, J. Deng, H. Su, J. Krause, S. Satheesh, S. Ma, Z. Huang, A. Karpathy, A. Khosla, M. Bernstein, et al., Imagenet large scale visual recognition challenge, *International Journal of Computer Vision* 115 (3) (2015) 211–252.
- [167] J. Folkesson, O. F. Olsen, P. Pettersen, E. Dam, C. Christiansen, Combining binary classifiers for automatic cartilage segmentation in knee mri, in: Y. Liu, T. Jiang, C. Zhang (Eds.), *Computer Vision for Biomedical Image Applications*, Springer Berlin Heidelberg, Berlin, Heidelberg, 2005, pp. 230–239.
- [168] J. Folkesson, E. B. Dam, O. F. Olsen, P. C. Pettersen, C. Christiansen, Segmenting articular cartilage automatically using a voxel classification approach, *IEEE transactions on medical imaging* 26 (1) (2007) 106–115.
- [169] E. B. Dam, J. Folkesson, M. Loog, P. Pettersen, C. Christiansen, Efficient automatic cartilage segmentation, in: MICCAI Joint Disease Workshop, 2006, pp. 88–95.
- [170] C. N. Öztürk, S. Albayrak, Automatic segmentation of cartilage in high-field magnetic resonance images of the knee joint with an improved voxel-classification-driven region-growing algorithm using vicinity-correlated subsampling, *Computers in biology and medicine* 72 (2016) 90–107.
- [171] E. B. Dam, M. Lillholm, J. Marques, M. Nielsen, Automatic segmentation of high-and low-field knee mris using knee image quantification with data from the osteoarthritis initiative, *Journal of Medical imaging* 2 (2) (2015) 024001–024001.
- [172] A. Prasoon, C. Igel, M. Loog, F. Lauze, E. Dam, M. Nielsen, Cascaded classifier for large-scale data applied to automatic segmentation of articular cartilage, in: *Medical Imaging 2012: Image Processing*, Vol. 8314, International Society for Optics and Photonics, 2012, pp. 83144–83149.
- [173] A. Prasoon, C. Igel, M. Loog, F. Lauze, E. B. Dam, M. Nielsen, Femoral cartilage segmentation in knee mri scans using two stage voxel classification, in: 2013 35th Annual International Conference of the IEEE Engineering in Medicine and Biology Society (EMBC), 2013, pp. 5469–5472.
- [174] S. Koo, B. Hargreaves, T. Andriacchi, G. Gold, Automatic segmentation of articular cartilage from mri: a multi-contrast and multi-dimensional approach, in: *Proc. Intl. Soc. Mag. Reson. Med*, Vol. 16, 2008, p. 2546.
- [175] S. Koo, B. A. Hargreaves, G. E. Gold, Automatic segmentation of articular cartilage from mri, uS Patent 8,706,188 (2014).
- [176] K. Zhang, J. Deng, W. Lu, Segmenting human knee cartilage automatically from multi-contrast mr images using support vector machines and discriminative random fields, in: 2011 18th IEEE International Conference on Image Processing, 2011, pp. 721–724.
- [177] K. Zhang, W. Lu, P. Marziliano, Automatic knee cartilage segmentation from multi-contrast mr images using support vector machine classification with spatial dependencies, *Magnetic resonance imaging* 31 (10) (2013) 1731–1743.
- [178] T. Joachims, Making large-scale SVM learning practical, in: B. Schölkopf, C. Burges, A. Smola (Eds.), *Advances in Kernel Methods - Support Vector Learning*, MIT Press, Cambridge, MA, 1999, Ch. 11, pp. 169–184.
- [179] Q. Wang, D. Wu, L. Lu, M. Liu, K. L. Boyer, S. K. Zhou, Semantic context forests for learning-based knee cartilage segmentation in 3d mr images, in: B. Menze, G. Langs, A. Montillo, M. Kelm, H. Müller, Z. Tu (Eds.), *Medical Computer Vision. Large Data in Medical Imaging*, Springer International Publishing, Cham, 2014, pp. 105–115.
- [180] Q. Liu, Q. Wang, L. Zhang, Y. Gao, D. Shen, Multi-atlas context forests for knee mr image segmentation, in: L. Zhou, L. Wang, Q. Wang, Y. Shi (Eds.), *Machine Learning in Medical Imaging*, Springer International Publishing, Cham, 2015, pp. 186–193.
- [181] A. Prasoon, K. Petersen, C. Igel, F. Lauze, E. Dam, M. Nielsen, Deep feature learning for knee cartilage segmentation using a triplanar convolutional neural network, in: K. Mori, I. Sakuma, Y. Sato, C. Barillot, N. Navab (Eds.), *Medical Image Computing and Computer-Assisted Intervention – MICCAI 2013*, Springer Berlin Heidelberg, Berlin, Heidelberg, 2013, pp. 246–253.
- [182] A. Tiulpin, J. Thevenot, E. Rahtu, P. Lehenkari, S. Saarakkala, Automatic knee osteoarthritis diagnosis from plain radiographs: A deep learning-based approach, *Scientific Reports* 8 (1) (2018) 1727.
- [183] N. Srivastava, G. Hinton, A. Krizhevsky, I. Sutskever, R. Salakhutdinov, Dropout: a simple way to prevent neural networks from overfitting, *The Journal of Machine Learning Research* 15 (1) (2014) 1929–1958.
- [184] H. C. Shin, H. R. Roth, M. Gao, L. Lu, Z. Xu, I. Noguees, J. Yao, D. Mollura, R. M. Summers, Deep convolutional neural networks for computer-aided detection: Cnn architectures, dataset characteristics and transfer learning, *IEEE Trans Med Imaging* 35 (5) (2016) 1285–1298.
- [185] B. Norman, V. Pedoia, S. Majumdar, Use of 2d u-net convolutional neural networks for automated cartilage and meniscus segmentation of knee mr imaging data to determine relaxometry and morphometry, *Radiology* 288 (1) (2018) 177–185.
- [186] O. Ronneberger, P. Fischer, T. Brox, U-net: Convolutional networks for biomedical image segmentation, in: N. Navab, J. Hornegger, W. M. Wells, A. F. Frangi (Eds.), *Medical Image Computing and Computer-Assisted Intervention – MICCAI 2015*, Springer International Publishing, Cham, 2015, pp. 234–241.
- [187] J. H. Kellgren, J. S. Lawrence, Radiological assessment of osteo-arthrosis, *Annals of the rheumatic diseases* 16 (4) (1957) 494–502.
- [188] F. Liu, Z. Zhou, H. Jang, A. Samsonov, G. Zhao, R. Kijowski, Deep convolutional neural network and 3d deformable approach for tissue segmentation in musculoskeletal magnetic resonance imaging, *Magnetic Resonance in Medicine* 79 (4) (2018) 2379–2391.

- [189] V. Badrinarayanan, A. Kendall, R. Cipolla, Segnet: A deep convolutional encoder-decoder architecture for image segmentation, arXiv preprint arXiv:1511.00561.
- [190] Z. Zhou, G. Zhao, R. Kijowski, F. Liu, Deep convolutional neural network for segmentation of knee joint anatomy, *Magnetic Resonance in Medicine* 0 (0) (2018) 1–12.
- [191] F. Ambellan, A. Tack, M. Ehlke, S. Zachow, Automated segmentation of knee bone and cartilage combining statistical shape knowledge and convolutional neural networks: Data from the osteoarthritis initiative, *Medical Image Analysis*.
- [192] Z. Quo, L. Zhang, L. Lu, M. Bagheri, R. M. Summers, M. Sonka, J. Yao, Deep logismos: Deep learning graph-based 3d segmentation of pancreatic tumors on ct scans, in: *Biomedical Imaging (ISBI 2018), 2018 IEEE 15th International Symposium on, IEEE, 2018*, pp. 1230–1233.